PAPER · **OPEN ACCESS**

Dynamical generation and transfer of nonclassical states in strongly interacting light-matter systems in cavities

To cite this article: Ilia Tutunnikov *et al* 2025 *Quantum Sci. Technol.* **10** 025002

IOP Publishing Quantum Sci. Technol. 10 (2025) 025002 https://doi.org/10.1088/2058-9565/ada2b8

Quantum Science and Technology

OPEN ACCESS

RECEIVED
2 October 2024

REVISED
17 December 2024

ACCEPTED FOR PUBLICATION
23 December 2024

PUBLISHED
9 January 2025

PAPER

Dynamical generation and transfer of nonclassical states in strongly interacting light-matter systems in cavities

Ilia Tutunnikov[1], **Vasil Rokaj**[1,2,3,*], **Jianshu Cao**[4] **and H R Sadeghpour**[1]

[1] ITAMP, Center for Astrophysics | Harvard & Smithsonian, Cambridge, MA 02138, United States of America
[2] Department of Physics, Villanova University, Villanova, PA 19085, United States of America
[3] Department of Physics, Harvard University, Cambridge, MA 02138, United States of America
[4] Department of Chemistry, Massachusetts Institute of Technology, Cambridge, MA 02139, United States of America
[*] Author to whom any correspondence should be addressed.

E-mail: vasil.rokaj@villanova.edu

Keywords: polaritons, cavity QED, quantum state transfer, nonclassical light, polaritonic technologies

Abstract

We propose leveraging strong and ultrastrong light-matter coupling to efficiently generate and exchange nonclassical light and quantum matter states. Two initial conditions are considered: (a) a displaced quadrature-squeezed matter state, and (b) a coherent state in a cavity. In both scenarios, polaritons mediate the dynamical generation and transfer of nonclassical states between light and matter. By monitoring the dynamics of both subsystems, we uncover the emergence of cavity-induced beatings in the collective matter oscillations. The beating period depends on the particle density through the vacuum Rabi splitting and peaks sharply under light-matter resonance conditions. For initial condition (a), nonclassicality is efficiently transferred from matter to photons under strong and ultrastrong coupling. However, for initial condition (b), nonclassical photonic states are generated only in the ultrastrong coupling regime due to the counter-rotating terms, highlighting the advantages of ultrastrong coupling. Furthermore, in the ultrastrong coupling regime, distinctive asymmetries relative to cavity detuning emerge in dynamical observables of both light and matter. The nonclassical photons can be extracted through a semi-transparent cavity mirror, while nonclassical matter states can be detected via time-resolved spectroscopy. This work highlights that polariton states may serve as a tool for dynamically generating and transferring nonclassical states, with potential applications in quantum technology.

1. Introduction

Strong light–matter interaction is essential for nascent quantum technologies, enabling efficient and reversible quantum state transfer, generation of correlated states, photon-mediated interactions, and nonclassical light. Under strong light-matter coupling, hybrid light-matter quasiparticles, known as polaritons, emerge [1]. These quasiparticles are often best manipulated in cavities [1–4], and have been widely studied in condensed matter [5–16], cold atoms [17–20], and molecular systems [21–31].

Polaritons inherit their attributes from their light and matter constituents and thus exhibit fascinating properties. In the strong coupling regime, photon emission statistics have been explored in ultracold atomic gases, leveraging strong Rydberg correlations for deterministic single-photon generation [18, 19]. Second-order photon correlation measurements confirm the quantum nature of emitted light, achieving high fidelity with high-finesse optical cavities [32]. Squeezed light [33] has been demonstrated in various optomechanical systems [34, 35], e.g. mechanical resonators [36, 37] and ultracold atoms [38].

This work explores the dynamic generation and transfer of nonclassical states of quantum matter and light. We leverage strong and ultrastrong light-matter coupling in single-mode cavities to achieve this [39, 40]. The dynamics of the composite system are described using the archetypical Hopfield Hamiltonian (HH), originally developed for studying the excitonic response in dielectric crystals [41]. We show that the HH applies to various physical systems in cavities, including cold, harmonically trapped ions [40],

two-dimensional (2D) electron gases in a strong magnetic field (Landau levels) [5–8, 12, 15], and oriented polar molecules [42, 43].

Trapped ions are ideal for studying quantum phenomena, and ion-cavity systems have enabled single-photon emission, ion-photon, and ion–ion entanglement [44–47]. The position of a trapped ion can be precisely controlled within the cavity [48] and Fock, coherent, and squeezed motional states of a harmonically trapped ion have been generated [49]. Coherent transfer between an ion's internal degrees of freedom and an optical cavity mode has been demonstrated in several experiments [50, 51]. However, cavity coupling with the motional states of trapped ions remains technically challenging due to the relatively low characteristic motional frequencies, often in the MHz range [47, 52].

Importantly, Landau levels exhibit ultrastrong coupling to the cavity field [4, 8–10, 12, 53–55] and Landau polaritons have been observed [7, 8, 12, 55–57]. More recently, mechanisms for cavity-induced modification of the integer Hall effect were proposed [58, 59], and the breakdown of topological protection has been experimentally demonstrated [5]. Furthermore, molecular polaritonic systems have garnered attention for modifying material properties, including chemical reactivity under vibrational strong coupling (VSC) [21, 22, 30, 60–64], and transient diffusivity and transport [28, 31, 65–72]. These findings have led to extensive theoretical and experimental work to elucidate the mechanisms behind the observed effects [24, 70, 73–76]. Despite important advances, the quantum nature of the observed phenomena remains an active area of research [77, 78].

This work focuses on the collective dynamics in cavity quantum electrodynamics (QED) systems by considering two schemes for the *generation and transfer of* nonclassical states of light and matter in a cavity. In **Scheme I**, the matter state, e.g. the center of mass (CM) state of trapped ions, is displaced and quadrature-squeezed. The dynamics of both subsystems are monitored, and we uncover the emergence of beatings in the collective matter oscillations and the number of generated photons. The beating period depends on the number of particles and the detuning, and it sharply peaks around the light-matter resonance. This phenomenon highlights that collective dynamics of matter can be significantly modified via strong and resonant light–matter interaction in a cavity, even without an external field, i.e. in a vacuum. Similar resonant modifications have been observed in chemical reactions in molecules under VSC [21, 22, 30, 63, 64]. From the cavity perspective, the coupling *transfers* the quantum state of matter (e.g. *motional* state of ions) to light, resulting in sub-Poissonian photon number distribution (PND), i.e. quantum photonic states with no classical analogue [79]. We wish to mention that generating nonclassical light via VSC with few molecules was suggested recently [80]. In **Scheme II**, the cavity is initiated in a coherent state [81], which partially moves from one subsystem to another over time. Simultaneously, the counter-rotating light–matter interaction terms (counter-rotating terms, CRT) in the HH (see below) induce nonclassical features in light or matter subsystems depending on the initial shift of the coherent state. In this scheme, the nonclassical features arise entirely from the CRT, underscoring the importance of the ultrastrong coupling [3, 4].

Notably, the CRT induce asymmetries in dynamical observables associated with matter and light. These asymmetries emerge in the ultrastrong coupling regime when the cavity frequency is scanned around the resonance and are consequences of the asymmetry in the polaritonic branches. In contrast to linear spectroscopy, which may be insensitive to the quantum nature of the system, time-dependent observables involving higher-order moments of the matter or light distributions (e.g. photon number variance) serve as quantum measures sensitive to ultrastrong coupling effects. We provide analytical expressions for the average photon number in both schemes, allowing for a comprehensive description of photon generation over the entire parameter space, including the system and initial state parameters.

We quantify the temporal evolution of nonclassical features of matter and light using the time-averaged Mandel Q parameter. For Scheme I, we demonstrate that outcoupling the cavity field through a semi-transparent cavity mirror allows for extracting the nonclassical photons [82]. In Scheme II applied to trapped ions, for instance, sideband spectroscopy of motional state population allows for the measurement of matter quantum state statistics [52]. Hybrid polaritonic systems efficiently mediate the transfer of nonclassicality from matter to light, a resource crucial for quantum sensing [83–86], and quantum information technologies [87, 88]. Our work bridges the physics of strong and ultrastrong light-matter coupling with quantum science and suggests novel pathways for polaritonic quantum technologies.

2. HH across different cavity QED systems

In recent years, the HH has attracted significant attention due to its application in several cavity QED systems operating in the ultrastrong light-matter coupling regime [3, 4]. This section explicitly demonstrates how the HH emerges in three example systems in a cavity: cold trapped ions, 2D electron gas in a strong magnetic field, and oriented molecules with harmonic internuclear potential. Thus, in principle, the nonclassical dynamical phenomena discussed hereafter are within experimental reach across various physical systems.

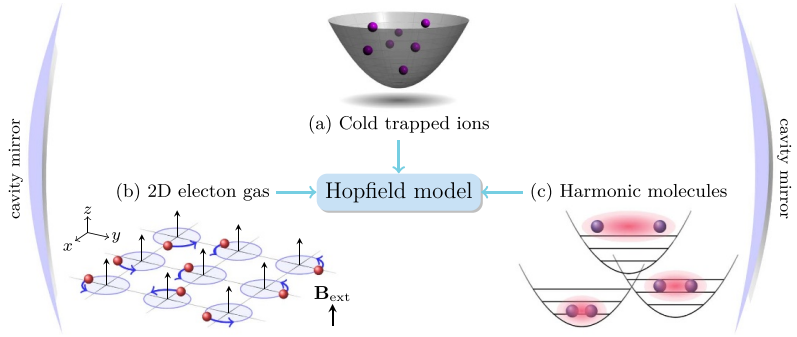

Figure 1. Schematic illustration of the collective coupling to a homogeneous quantum cavity field in different physical systems, including (a) harmonically trapped cold ions, (b) 2D electron gas in a strong magnetic field, $\mathbf{B}_{\text{ext}}$, and (c) molecules with harmonic internuclear potential. In all cases, the system Hamiltonian can be mapped to the HH, see equations (5), (10) and (14). Thus, the dynamical phenomena described hereafter can be, in principle, realized in various cavity QED systems.

2.1. Cold trapped ions

We start by considering a system of N interacting ions confined in a harmonic potential, coupled to a single-mode quantized cavity field (figure 1(a)). Recently, this system was used to study the collective phenomena in the polaritonic ground state [40]. Here, we focus on the dynamics mediated by the coupling between the ions' motion and the cavity field. In the non-relativistic limit, this system is described by the Pauli–Fierz Hamiltonian in the Coulomb gauge, also known as the minimal-coupling Hamiltonian [43, 89]

$$\hat{H}_{\text{ion}} = \frac{1}{2m}\sum_{i=1}^{N}\left(i\hbar\boldsymbol{\nabla}_i + g_0\hat{\mathbf{A}}\right)^2 + \sum_{i<l}^{N} W(\hat{\mathbf{r}}_i - \hat{\mathbf{r}}_l) + \sum_{i=1}^{N}\frac{m\Omega^2}{2}\hat{\mathbf{r}}_i^2 + \sum_{\nu=x,y}\hbar\omega\left(\hat{a}_\nu^\dagger\hat{a}_\nu + \frac{1}{2}\right), \tag{1}$$

where g_0 is the single-particle coupling parameter to the cavity field (in units of the elementary charge, e), m is the mass of the particles, and Ω is the frequency of the harmonic trap. $W(\hat{\mathbf{r}}_i - \hat{\mathbf{r}}_l)$ is the inter-particle interaction between the ions. The quantized vector potential $\hat{\mathbf{A}}$ in the long-wavelength limit (homogeneous approximation) is given by [42, 43, 89]

$$\hat{\mathbf{A}} = \sum_{\nu=x,y}\sqrt{\frac{\hbar}{2\epsilon_0\mathcal{V}\omega}}\mathbf{e}_\nu\left(\hat{a}_\nu + \hat{a}_\nu^\dagger\right), \tag{2}$$

where $\omega = c|k_z|$ is the frequency in the effective optical mode volume $\mathcal{V}$, with wave vector in the z direction, ϵ_0 is the vacuum permittivity, and $\nu = x, y$ denote the two transversal polarization directions [43, 89]. The operators $\hat{a}_\nu$ and $\hat{a}_\nu^\dagger$ are the annihilation and creation operators of the photon field obeying $[\hat{a}_\nu, \hat{a}_{\nu'}{}^\dagger] = \delta_{\nu\nu'}$.

Expanding the covariant kinetic energy shows that the homogeneous photon field couples to the total momentum of the particles, $\hat{\mathbf{A}}\cdot\sum_{i=1}^{N}\nabla_i$, implying *collective* coupling to the cavity field through the particles' center of mass. Thus, we change variables to the CM position $\hat{\mathbf{R}} = N^{-1/2}\sum_{i=1}^{N}\hat{\mathbf{r}}_i$, and the relative positions $\hat{\tilde{\mathbf{r}}}_j = N^{-1/2}(\hat{\mathbf{r}}_1 - \hat{\mathbf{r}}_j)$ with $j > 1$. The prefactor $N^{-1/2}$ is introduced for mathematical convenience like in [90]. The operators $\hat{\mathbf{R}}$ and $\hat{\tilde{\mathbf{r}}}_j$, along with their corresponding momenta commute. This confirms the independence of CM and relative coordinates (appendix A.1).

The scalar trapping potential separates into two parts: the first depends on the CM coordinate, while the second depends on the relative coordinates without cross-terms between the two, $\sum_{i=1}^{N}\hat{\mathbf{r}}_i^2 = \hat{\mathbf{R}}^2 + N\sum_{j=2}^{N}\hat{\tilde{\mathbf{r}}}_j^2 - (\sum_{j=2}^{N}\hat{\tilde{\mathbf{r}}}_j)^2$. The two-body interaction $W(\hat{\mathbf{r}}_i - \hat{\mathbf{r}}_l)$ depends only on the relative distances, so it does not affect the cavity-induced CM motion. The Hamiltonian, therefore, splits into two parts: (i) $\hat{H}_{\text{ion-cm}}$, describing the CM coupling to the quantized field $\hat{\mathbf{A}}$,

$$\hat{H}_{\text{ion-cm}} = \frac{1}{2m}\left(i\hbar\nabla_{\mathbf{R}} + g_0\sqrt{N}\hat{\mathbf{A}}\right)^2 + \frac{m\Omega^2}{2}\hat{\mathbf{R}}^2 + \sum_{\nu=x,y}\hbar\omega\left(\hat{a}_\nu^\dagger\hat{a}_\nu + \frac{1}{2}\right), \tag{3}$$

and (ii) $\hat{H}_{\text{ion-rel}}$ (presented in appendix A.1), describing the dynamics of the relative coordinates, decoupled from both $\hat{\mathbf{A}}$ and the CM. We now focus on the dynamics of the CM degree of freedom coupled to the cavity

described by $\hat{H}_{\text{ion-cm}}$. Since the polarization vectors of the photon field lie in the (x, y) plane, the z direction is trivial, while x and y are independent,

$$\hat{H}_{\text{ion-cm}} = \sum_{\nu=x,y}\left[-\frac{\hbar^2}{2m}\partial^2_{R_\nu} + \frac{\mathrm{i}g_0\hbar}{m}\sqrt{N}\hat{A}_\nu\partial_{R_\nu} + \frac{m\Omega^2}{2}\hat{R}^2_\nu + \frac{Ng_0^2}{2m}\hat{A}^2_\nu + \hbar\omega\left(\hat{a}^\dagger_\nu\hat{a}_\nu + \frac{1}{2}\right)\right]. \tag{4}$$

To avoid any confusion, note that $\hat{\mathbf{R}} = (\hat{R}_x, \hat{R}_y) = (\hat{X}, \hat{Y})$, $\nabla_{\mathbf{R}} = (\partial_{R_x}, \partial_{R_y}) = (\partial_X, \partial_Y)$ and $\hat{\mathbf{A}} = (\hat{A}_x, \hat{A}_y)$. Without loss of generality, we focus on the X component of the Hamiltonian. We also suppress the x index in the photon operators for simplicity, i.e. $\hat{a} \equiv \hat{a}_x$. Finally, to simplify the Hamiltonian, we introduce bosonic operators for matter $\hat{b} = \sqrt{m\Omega/(2\hbar)}[\hat{X} + \hbar/(m\Omega)\partial_X]$. The CM Hamiltonian turns into the well-known HH [3, 41]

$$\hat{H}_{\text{ion-cm}} = \hbar\Omega\left(\hat{b}^\dagger\hat{b} + \frac{1}{2}\right) + \mathrm{i}\hbar\sqrt{\frac{\Omega g_0^2 N}{4m\epsilon_0\mathcal{V}\omega}}\left(\hat{a} + \hat{a}^\dagger\right)\left(\hat{b} - \hat{b}^\dagger\right) + \frac{\hbar N g_0^2}{4m\epsilon_0\mathcal{V}\omega}\left(\hat{a} + \hat{a}^\dagger\right)^2 + \hbar\omega\left(\hat{a}^\dagger\hat{a} + \frac{1}{2}\right). \tag{5}$$

2.2. 2D electron gas

Next, we consider 2D electron gas (2deg) subject to a homogeneous magnetic field perpendicular to the plane. The electrons are also coupled to a homogeneous single-mode cavity field (figure 1(b)). Landau-level systems in a cavity have been theoretically studied and experimentally realized [7, 8, 15]. Many interesting phenomena have been observed, including Landau polariton quasiparticles and modifications of quantum Hall transport [5, 6, 8, 12]. The Hamiltonian for the quantum Hall system in the cavity is given by

$$\hat{H}_{\text{2deg}} = \frac{1}{2m}\sum_{i=1}^{N}\left(\hat{\boldsymbol{\pi}}_i + e\hat{\mathbf{A}}\right)^2 + \sum_{i<l}^{N} W(\hat{\mathbf{r}}_i - \hat{\mathbf{r}}_l) + \hbar\omega\left(\hat{a}^\dagger\hat{a} + \frac{1}{2}\right), \tag{6}$$

where $\hat{\boldsymbol{\pi}}_i = \mathrm{i}\hbar\nabla_i + e\mathbf{A}_{\text{ext}}(\hat{\mathbf{r}}_i)$ are the dynamical momenta, and $\mathbf{A}_{\text{ext}}(\hat{\mathbf{r}}) = -\mathbf{e}_y B\hat{x}$ describes the magnetic field $\mathbf{B} = \nabla \times \mathbf{A}_{\text{ext}}(\hat{\mathbf{r}}) = B\mathbf{e}_z$. The cavity field $\hat{\mathbf{A}} = \sqrt{\hbar/(2\epsilon_0\mathcal{V}\omega)}\mathbf{e}_y(\hat{a} + \hat{a}^\dagger)$ is characterized by the in-plane polarization vector $\mathbf{e}_y$ and the photon's bare frequency ω. Further, $W(\hat{\mathbf{r}}_i - \hat{\mathbf{r}}_j) = (4\pi\epsilon_0)^{-1}|\hat{\mathbf{r}}_i - \hat{\mathbf{r}}_j|$ is the Coulomb interaction between the electrons. The transformations of momenta $\{\nabla_i\}$ and the two-body interaction are described in appendix A.1.

The interaction between the cavity field and the electrons is given by $\hat{\mathbf{A}} \cdot \sum_{i=1}^{N} \mathrm{i}\hbar\nabla_i + e\mathbf{A}_{\text{ext}}(\hat{\mathbf{r}}_i) = \sqrt{N}\hat{\mathbf{A}} \cdot [\mathrm{i}\hbar\nabla_{\mathbf{R}} + e\mathbf{A}_{\text{ext}}(\hat{\mathbf{R}})]$, such that the cavity field couples only to the CM of the 2deg (appendix A.2). After the transformation, the Hamiltonian is given by $\hat{H}_{\text{2deg}} = \hat{H}_{\text{2deg-cm}} + \hat{H}_{\text{2deg-rel}}$, where $\hat{H}_{\text{2deg-cm}}$ includes the coupling to the quantized field, $\hat{\mathbf{A}}$, while $\hat{H}_{\text{2deg-rel}}$ depends on the relative distances and is decoupled from $\hat{\mathbf{A}}$. The CM part, governing the light-matter dynamics, is given by

$$\hat{H}_{\text{2deg-cm}} = \frac{1}{2m}\left(\mathrm{i}\hbar\nabla_{\mathbf{R}} + e\mathbf{A}_{\text{ext}}\left(\hat{\mathbf{R}}\right) + e\sqrt{N}\hat{\mathbf{A}}\right)^2 + \hbar\omega\left(\hat{a}^\dagger\hat{a} + \frac{1}{2}\right). \tag{7}$$

The expression for $\hat{H}_{\text{2deg-rel}}$ is presented in the appendix A.2. In the Landau gauge, the Hamiltonian is translationally invariant along the y axis. Thus, the eigenfunctions related to this direction in space are plane waves of the form $\exp(\mathrm{i}K_y\hat{Y})$. Applying $\hat{H}_{\text{2deg-cm}}$ to the plane wave and introducing the shifted coordinate $\hat{\bar{X}} = \hat{X} + \hbar K_y/eB$, the Hamiltonian becomes

$$\hat{H}_{\text{2deg-cm}} = -\frac{\hbar^2}{2m}\frac{\partial^2}{\partial\bar{X}^2} + \frac{m\omega_c^2}{2}\hat{\bar{X}}^2 - \frac{e^2B\sqrt{N}}{m}\hat{A}\hat{\bar{X}} + \frac{e^2N}{2m}\hat{A}^2 + \hbar\omega\left(\hat{a}^\dagger\hat{a} + \frac{1}{2}\right), \tag{8}$$

where, $\omega_c = eB/m$ is the cyclotron frequency. To simplify the Hamiltonian further, we perform a Fourier transformation on the electronic coordinate $\phi(\hat{\bar{X}}) = (2\pi)^{-1}\int_{-\infty}^{\infty}\tilde{\phi}(\hat{K})\exp(-\mathrm{i}\hat{K}\hat{\bar{X}})\,\mathrm{d}\hat{K}$, such that

$$\hat{H}_{\text{2deg-cm}} = -\frac{m\omega_c^2}{2}\frac{\partial^2}{\partial K^2} + \frac{\hbar^2}{2m}\hat{K}^2 + \mathrm{i}\frac{e^2B\sqrt{N}}{m}\hat{A}\partial_K + \frac{e^2N}{2m}\hat{A}^2 + \hbar\omega\left(\hat{a}^\dagger\hat{a} + \frac{1}{2}\right). \tag{9}$$

Finally, to turn $\hat{H}_{\text{2deg-cm}}$ into HH form, we introduce annihilation and creation operators $\{\hat{l}, \hat{l}^\dagger\}$ for the matter degrees of freedom $\hat{K} = \sqrt{m\omega_c/(2\hbar)}(\hat{l} + \hat{l}^\dagger)$ and $\partial_K = \sqrt{\hbar/(2m\omega_c)}(\hat{l} - \hat{l}^\dagger)$, such that

$$\hat{H}_{\text{2deg-cm}} = \hbar\omega_c\left(\hat{l}^\dagger\hat{l} + \frac{1}{2}\right) + \mathrm{i}\hbar\sqrt{\frac{e^2N\omega_c}{4m\epsilon_0\mathcal{V}\omega}}\left(\hat{a} + \hat{a}^\dagger\right)\left(\hat{l} - \hat{l}^\dagger\right) + \frac{\hbar e^2 N}{4m\epsilon_0\mathcal{V}\omega}\left(\hat{a} + \hat{a}^\dagger\right)^2 + \hbar\omega\left(\hat{a}^\dagger\hat{a} + \frac{1}{2}\right). \tag{10}$$

Thus, the CM Hamiltonian for Landau levels coupled to the cavity assumes the same mathematical form as that of harmonically trapped ions, with one important difference. Since we applied a Fourier transformation to the matter operators to arrive at equation (10), the dynamical phenomena that occur in real space for the ions manifest in k-space for the Landau levels.

2.3. Harmonic molecules

As an additional example, we consider a system of N identical non-interacting polar molecules collectively coupled to a single-mode cavity. The molecular vibrations are described by one-dimensional harmonic potential. For simplicity, the molecules are assumed to be oriented along one of the cavity polarization directions. For the molecular system, we use the length gauge form of the Pauli–Fierz Hamiltonian [42, 43], which, given these assumptions, takes the form

$$\hat{H}_{\rm mol} = \sum_{i=1}^{N}\left[-\frac{\hbar^2}{2M}\frac{\partial^2}{\partial x_i^2} + \frac{M\Omega_{\rm vib}^2}{2}\hat{x}_i^2\right] + \hbar\omega\left[-\frac{1}{2}\frac{\partial^2}{\partial q^2} + \frac{1}{2}\left(\hat{q} - g\sum_{i=1}^{N}\hat{x}_i\right)^2\right]. \tag{11}$$

Here, $\Omega_{\rm vib}$ is the fundamental frequency of the harmonic potential, M is the molecular mass, and ω is the cavity frequency. $g = \mu_0/\sqrt{\omega\epsilon_0\mathcal{V}}$ is the light-molecule coupling constant, which depends on the effective optical mode volume $\mathcal{V}$, the vacuum permittivity ϵ_0, and the magnitude of the molecular dipole moment, μ_0. The operators $\hat{q}$ and ∂_q describe the position and momentum quadratures of the bosonic cavity mode. However, they should not be confused with the creation and annihilation photon operators $\hat{a}^\dagger, \hat{a}$ in the Coulomb gauge, as their connection is subtle [91].

The model Hamiltonian $\hat{H}_{\rm mol}$ has been used in multiple works studying molecular systems under VSC in cavities [24, 75, 76, 92, 93]. The perfectly oriented molecules couple to the cavity through the collective dipole moment. Thus, we transform $\hat{H}_{\rm mol}$ into the CM frame by introducing the CM coordinate $\hat{X} = (N)^{-1/2}\sum_i \hat{x}_i$ and the relative bond lengths $\hat{\tilde{x}}_j = (\hat{x}_1 - \hat{x}_j)/\sqrt{N}$ with $j > 1$. We already showed how the kinetic energy terms and the harmonic potential transform into the CM frame in appendix A.1. Thus, it is straightforward to obtain the CM Hamiltonian, while the relative bond lengths Hamiltonian separates out like in the previous models,

$$\begin{aligned}
\hat{H}_{\text{mol-cm}} &= -\frac{\hbar^2}{2M}\frac{\partial^2}{\partial X^2} + \frac{M\Omega_{\rm vib}^2}{2}\hat{X}^2 + \hbar\omega\left[-\frac{1}{2}\frac{\partial^2}{\partial q^2} + \frac{1}{2}\left(\hat{q} - g\sqrt{N}\hat{X}\right)^2\right], \\
\hat{H}_{\text{mol-rel}} &= -\frac{\hbar^2}{2MN}\sum_{j=2}^{N}\partial_{\tilde{x}_j}^2 - \frac{\hbar^2}{2MN}\sum_{j,k=2}^{N}\partial_{\tilde{x}_j}\cdot\partial_{\tilde{x}_k} + \frac{MN\Omega_{\rm vib}^2}{2}\sum_{j=2}^{N}\hat{\tilde{x}}_j^2 - \frac{M\Omega_{\rm vib}^2}{2}\left[\sum_{j=2}^{N}\hat{\tilde{x}}_j\right]^2.
\end{aligned} \tag{12}$$

The cavity mode quadrature, $\hat{q}$, couples only to the CM coordinate $\hat{X}$ in $\hat{H}_{\text{mol-cm}}$. We next expand $(\hat{q} - g\sqrt{N}\hat{X})^2$ and apply Fourier transformation to $\hat{q}$, $\phi(\hat{q}) = (2\pi)^{-1}\int_{-\infty}^{\infty}\tilde{\phi}(\hat{p})\exp(\mathrm{i}\hat{p}\hat{q})\,\mathrm{d}\hat{p}$. We find that the cavity-molecules CM Hamiltonian has the same mathematical form as the previously discussed two models,

$$\hat{H}_{\text{mol-cm}} = -\frac{\hbar^2}{2M}\frac{\partial^2}{\partial X^2} + \frac{M\Omega_{\rm vib}^2}{2}\hat{X}^2 + \frac{\hbar\omega g^2 N}{2}\hat{X}^2 + \mathrm{i}\hbar\omega g\sqrt{N}\hat{X}\frac{\partial}{\partial p} + \hbar\omega\left(-\frac{1}{2}\frac{\partial^2}{\partial p^2} + \frac{\hat{p}^2}{2}\right). \tag{13}$$

Finally, we can write the above Hamiltonian in terms of annihilation and creation operators, $\hat{m} = \sqrt{M\Omega_{\rm vib}/(2\hbar)}[\hat{X} + \hbar/(M\Omega_{\rm vib})\partial_X]$ for matter, and $\hat{c} = (\hat{p} + \partial_p)/\sqrt{2}$ for light,

$$\hat{H}_{\text{mol-cm}} = \hbar\Omega_{\rm vib}\left(\hat{m}^\dagger\hat{m} + \frac{1}{2}\right) + \mathrm{i}\hbar\omega g\sqrt{\frac{\hbar N}{4M\Omega_{\rm vib}}}\left(\hat{m}^\dagger + \hat{m}\right)\left(\hat{c} - \hat{c}^\dagger\right) + \frac{\hbar^2\omega g^2 N}{4M\Omega_{\rm vib}}\left(\hat{m}^\dagger + \hat{m}\right)^2 + \hbar\omega\left(\hat{c}^\dagger\hat{c} + \frac{1}{2}\right). \tag{14}$$

The molecule-cavity Hamiltonian above has the standard form of the HH [41]. However, the bosonic quadratic term appears for the matter operators $\hat{m}$, $\hat{m}^\dagger$. Thus, the dynamics that appear for photons in the ion-cavity system will manifest for the matter in the molecule-cavity system.

2.4. HH for the CM and polariton modes

In the previous subsections, we demonstrated that, across three cavity QED platforms, the collective coupling of an ensemble of particles (ions, 2degs, molecules) is described by the HH in equation (5). In all cases, the bosonic/harmonic matter part is given by $\sim\hbar\Omega\hat{b}^\dagger\hat{b}$, the cavity mode is described by $\sim\hbar\omega\hat{a}^\dagger\hat{a}$, the bilinear interaction is $\sim\sqrt{N}(\hat{a} + \hat{a}^\dagger)(\hat{b} - \hat{b}^\dagger)$. The last term is the quadratic photon self-interaction in the Coulomb gauge, $\sim N(\hat{a} + \hat{a}^\dagger)^2$, or the matter self-interaction, $\sim N(\hat{m} + \hat{m}^\dagger)^2$, in the length gauge.

In what follows, we examine the dynamics of the HH, focusing on trapped ions for concreteness, as this system is more intuitive than 2D electron gas (Landau levels) or molecules. We assume a Fabry–Pérot cavity consists of two flat parallel mirrors with area $\mathcal{A}$, separated by a distance L, giving the effective optical mode volume $\mathcal{V} = \mathcal{A}L/2$. The effective mode volume differs from the geometric volume due to the spatial distribution of the field in the cavity [94]. From this, the dimensionless form of equation (5) is given by

$$\hat{\mathcal{H}} = \frac{1}{2}\left(\hat{P}^2 + \hat{X}^2\right) + \frac{\gamma}{2}\left(\hat{p}^2 + \hat{q}^2\right) - \lambda\hat{q}\hat{P} + \frac{\lambda^2}{2}\hat{q}^2, \tag{15}$$

where $\hat{X} \equiv (\hat{b}^\dagger + \hat{b})/\sqrt{2}$ and $\hat{P} \equiv \mathrm{i}(\hat{b}^\dagger - \hat{b})/\sqrt{2}$ are the CM position and momentum operators ($b^\dagger$ and b are the corresponding creation and annihilation operators), $\hat{q} \equiv (\hat{a}^\dagger + \hat{a})/\sqrt{2}$, $\hat{p} \equiv \mathrm{i}(\hat{a}^\dagger - \hat{a})/\sqrt{2}$ represent the position and momentum field quadratures. Energy, time, length, and momentum are measured in units of $\hbar\Omega$, $1/\Omega$, $\sqrt{\hbar/(m\Omega)}$, and $\sqrt{\hbar m\Omega}$, respectively. The field quadratures associated with position and momentum are measured in units of $\sqrt{\hbar/(\epsilon_0\mathcal{V}\Omega)}$ and $\sqrt{\hbar\epsilon_0\mathcal{V}\Omega}$, respectively. The two, dimensionless control parameters of $\hat{\mathcal{H}}$ are the frequency ratio between the cavity and the CM matter excitations, γ, and the collective coupling constant, λ, defined as [40]

$$\gamma \equiv \frac{\omega}{\Omega}, \qquad \lambda \equiv \sqrt{\frac{2Ng_0^2}{\pi\epsilon_0 c\mathcal{A}m\Omega}}, \tag{16}$$

where we define the fundamental cavity frequency, $\omega = \pi c/L$. The two polariton branches have energies $\Omega_\pm$, given by [40]

$$\Omega_\pm^2 = \frac{1+\gamma^2+\gamma\lambda^2}{2} \pm \frac{1}{2}\sqrt{(1+\gamma^2+\gamma\lambda^2)^2 - 4\gamma^2}. \tag{17}$$

The cavity resonates with the CM matter excitations at $\gamma = 1$. Appendix B shows the λ,γ-dependence of $\Omega_\pm$.

We numerically solve the time-dependent Schrödinger equation with $\hat{\mathcal{H}}$ to study the light-matter dynamics. We also employ a semi-classical analysis to derive exact analytical expressions for the observables. This approach relies on solving Hamilton's equations of motion, derived from the classical equivalent of $\hat{\mathcal{H}}$, for $X(t)$, $P(t)$, $q(t)$, and $p(t)$, and provides further insight into the underlying dynamics of the coupled system (appendix C). According to the Ehrenfest theorem, in a harmonic system, the first moments (e.g. $\langle\hat{X}(t)\rangle$, $\langle\hat{q}(t)\rangle$, etc) match the corresponding classical solutions exactly [95, 96]. Position-momentum uncertainty manifests in higher-order observables (e.g. $\langle\hat{X}^2\rangle$, $\langle\hat{P}^2\rangle$, $\langle\hat{q}^2\rangle$, etc). These observables are obtained by averaging classical expressions over the initial phase space distribution, corresponding to the composite system initial wave function. The Mandel Q functions of matter or light, which quantify deviations from classicallity, are obtained using fully quantum simulations.

3. Scheme I. Transfer of nonclassicality from matter to light

The transfer of nonclassical states is demonstrated by initializing the composite system with the matter CM displaced by X_0 and quadrature-squeezed in X, while the cavity is in the vacuum state. The initial wave function of the composite system is given by $\psi_0(X,q) \propto \exp[-(X-X_0)^2/(2w^2)]\exp(-q^2/2)$, where w is the width of the matter wave function. For $w = 1$, the matter is in its ground state, and for $w < 1$, it is quadrature-squeezed. Creation of coherent and quadrature-squeezed states of trapped ions has been demonstrated, e.g. in [49].

Generally, Scheme I relies on transferring non-classical matter states, such as the shifted and squeezed state of the CM of trapped ions, as described above. As we show later, under ultra-strong coupling, even shifted and unsqueezed states develop non-classicality. Shifted Landau levels can be realized using a constant electric field modeled as the scalar electric potential of the form $V_E(\mathbf{r}) = eEy$. Such potential shifts the electronic momenta in the y direction $k_y \to k_y + m_eE/(\hbar B)$ and the corresponding Landau levels wave functions [97]. Squeezing of the Landau levels can also be realized. The magnetic field B defines the frequency of the effective harmonic potential (via ω_c, see equation (10)). Thus, a squeezed state can be prepared by a sudden quench of the magnetic field. This might be experimentally challenging due to the magnitude of the typical magnetic fields. Alternatively, squeezing is possible in parabolic quantum wells as the ones used in quantum wires (2D) and quantum dots (3D) [98], or in semiconductor (GaAs or AlGaAs) quantum wells [99]. For oriented molecules, the required initial states can be prepared with coherent control schemes using pulsed lasers [100, 101].

The wave function ψ_0 corresponds to the semi-classical phase space distribution

$$\mathcal{P}(0) = \frac{1}{\pi^2}\exp\left[-\frac{(X(0)-X_0)^2}{w^2} - w^2P^2(0)\right]\exp\left[-q^2(0) - p^2(0)\right], \tag{18}$$

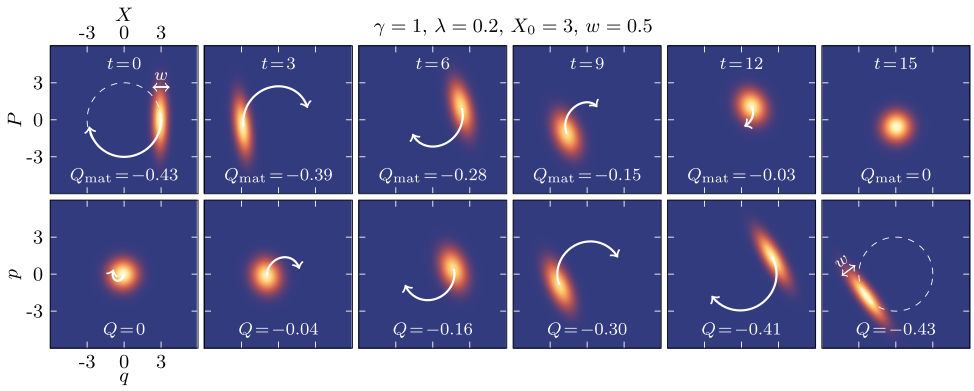

Figure 2. Snapshots of time evolution of the matter $(X, P$, upper row) and cavity states $(q, p$, bottom row) in their respective phase spaces. The initial state in Scheme I is a product of a displaced quadrature-squeezed matter CM state and cavity ground state (see equation (18)). Arrows indicate the trajectories of the phase space distribution centers. Initially, the radius of the trajectory equals the initial matter CM quadrature shift, X_0. The dimensional units for the variables and parameters in this work are defined after equation (15).

with $X(0)$, $P(0)$, $q(0)$, and $p(0)$ representing the initial conditions. Figure 2 presents a sequence of phase space snapshots for the light and matter subsystems. The initial state parameters are $X_0 = 3$ and $w = 0.5$, with light and matter at resonance ($\gamma = 1$), in the ultrastrong coupling regime ($\lambda = 0.2$).

On short timescales, the squeezed matter phase space distribution rotates counterclockwise at a radial distance of approximately X_0 while maintaining its elongated shape. As time progresses, the distribution becomes circularly symmetric and converges toward the origin. The motion of the phase space distribution has two characteristic frequencies defined by the polariton energies in equation (17): fast angular (or rotational) frequency, proportional to $\Omega_+ + \Omega_-$, and slow radial oscillation frequency, proportional to the vacuum Rabi splitting (VRS) $\bar{\Delta} \equiv \Omega_+ - \Omega_-$.

The matter CM dynamics, mediated by the light-matter coupling, generates photons, and the nonclassical state of matter effectively transfers to the light. The transfer occurs on the time scale of slow radial oscillation ($\bar{\Delta}^{-1}$), as illustrated in the bottom row in figure 2. The light distribution shifts away from the origin and becomes squeezed, mirroring the initial state of the matter. At resonance, a complete transfer does not require ultrastrong light–matter interaction, but the transfer *rate* is defined by the coupling strength, $\bar{\Delta} = \lambda$.

More generally, the phase space distributions here are multivariate Gaussians, appearing as rotated ellipses centered around $(\langle\hat{X}(t)\rangle, \langle\hat{P}(t)\rangle)$ or $(\langle\hat{q}(t)\rangle, \langle\hat{p}(t)\rangle)$. The eigenvectors of the covariance matrix define the orientation of the ellipses while the aspect ratio is proportional to the ratio of the eigenvalues (appendix D).

The Mandel Q function measures the deviation of PND from the Poisson distribution and is defined as [79, 102]

$$Q \equiv \frac{\langle(\Delta\hat{n})^2\rangle - \langle\hat{n}\rangle}{\langle\hat{n}\rangle}, \tag{19}$$

where $\hat{n} = \hat{a}^\dagger\hat{a} = (\hat{q}^2 + \hat{p}^2)/2 - 1/2$, and $\langle(\Delta\hat{n})^2\rangle \equiv \langle\hat{n}^2\rangle - \langle\hat{n}\rangle^2$. For $Q = 0$, photons are in a coherent state and obey trivial Poisson statistics, while for $Q > 0$, they obey super-Poissonian statistics, which have a classical analogue. When $Q < 0$, the photons follow sub-Poissonian statistics, a hallmark of quantum light with no classical counterpart [79, 102, 103]. Under certain conditions–specifically, in a single-mode cavity when the field is in a stationary state, the Mandel Q function is related to the zero-time-delay second-order correlation function $g^{(2)}(0)$ by $Q = \langle\hat{n}\rangle[g^{(2)}(0) - 1]$ [79, 104]. The quantity $g^{(2)}(0)$ is frequently used to infer photon correlations and quantifies the likelihood of simultaneous photon detection events.

Note that quadrature squeezing without displacement in the phase space does not result in sub-Poissonian statistics [79]. Geometrically, $\langle(\Delta\hat{n})^2\rangle \leqslant \langle\hat{n}\rangle$ occurs when the radial variance of the phase space distribution is lower than the average radial displacement. In figure 2, the *matter* is initially squeezed with $Q_{\rm mat} < 0$. Note that $Q_{\rm mat}$ is also defined by equation (19), but with $\hat{n}_{\rm mat} = \hat{b}^\dagger\hat{b} = (\hat{X}^2 + \hat{P}^2)/2 - 1/2$ being the number operator for the matter CM states. While matter and light states exchange, the nonclassical features emerge in the light degree of freedom, manifesting in $Q < 0$. The effective transfer of the matter state, characterized by a negative Q parameter, into the cavity mode is one of the key findings of this work.

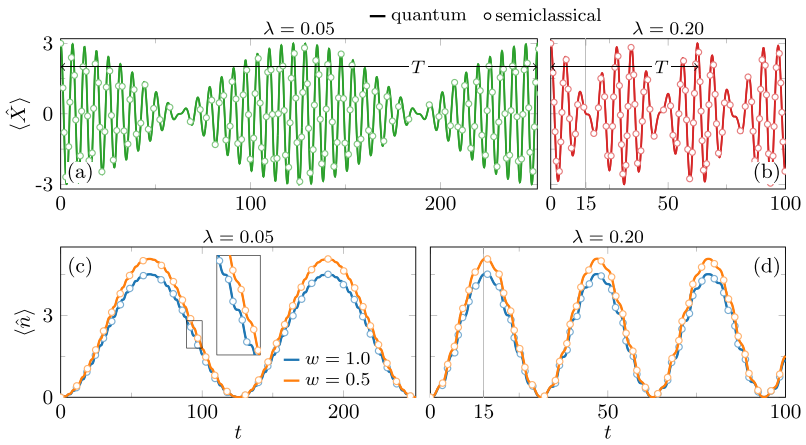

Figure 3. (a) and (b) Expectation values of the matter CM quadrature at resonance, $\langle \hat{X}(t) \rangle$ (see equation (20), $\gamma = 1$, $X_0 = 3$, $w = 0.5$) for two light-matter coupling regimes, strong ($\lambda = 0.05$) and ultrastrong ($\lambda = 0.2$). $\langle \hat{X}(t) \rangle$ is independent of w. The beating period is defined as $T \equiv 2\pi/(\bar{\Delta}/2)$, while the period of the high-frequency oscillations is given by $2\pi/(\bar{\Sigma}/2)$. At resonance, $\bar{\Delta} = \lambda$, and $T = 4\pi/\lambda \approx 251,63$ for (a) and (b), respectively, illustrating the strong dependence on the collective coupling, λ. (c) and (d) The generated photon number expectation values at resonance for squeezed and non-squeezed matter initial states. The inset in (c) shows the presence of high-frequency oscillations. The quantum and semiclassical results agree in all cases.

3.1. Beating and light-matter resonance

Next, we explore the dynamics of the subsystems in more detail. Figures 3(a) and (b) shows the expectation value of the matter CM position quadrature, $\langle \hat{X}(t) \rangle$, at resonance with the cavity ($\gamma = 1$), in strong (ultrastrong) light-matter coupling regime, $\lambda = 0.05$ ($\lambda = 0.2$). According to the Ehrenfest theorem [95, 96], $\langle \hat{X}(t) \rangle$ equals the classical solution $X(t)$ of a single particle with initial position X_0, and zero momentum (appendix C)

$$\frac{\langle \hat{X}(t) \rangle}{X_0} = \cos\left[\frac{\bar{\Sigma}t}{2}\right]\cos\left[\frac{\bar{\Delta}t}{2}\right] + \beta \sin\left[\frac{\bar{\Sigma}t}{2}\right]\sin\left[\frac{\bar{\Delta}t}{2}\right], \tag{20}$$

where $\bar{\Sigma} \equiv \Omega_+ + \Omega_-$, $\bar{\Delta} \equiv \Omega_+ - \Omega_- = \sqrt{(1-\gamma)^2 + \gamma\lambda^2}$ is the VRS, $\bar{\Delta} \leqslant \bar{\Sigma}$, and $\beta = (\Omega_+^2 + \Omega_-^2 - 2)/(\bar{\Sigma}\bar{\Delta})$. The higher frequency, $\bar{\Sigma}$, defines the rotation period of the phase space distributions in figure 2. The VRS, on the other hand, defines the long beating period $T = 2\pi/(\bar{\Delta}/2)$ during which $\langle \hat{X} \rangle$ exhibits slow beatings, and state transfer occurs. This emergent long timescale, inversely proportional to the VRS, depends on the collective coupling and, consequently, the number of particles, $\lambda \propto \sqrt{N}$ (at resonance, $\bar{\Delta} = \lambda$).

In addition to the collective nature of the beating phenomenon, it is important to highlight the dependence of T on the detuning. In figure 4(c), we observe that when light and matter excitations are in resonance ($\gamma = 1$), the beating period reaches its maximum. This shows that the collective dynamics of an ensemble of particles resonantly coupled to a cavity can be significantly modified even in a vacuum i.e. without an external driving field. Similar modifications of dynamics at resonance have been observed in chemical reactions of collectively coupled molecules under VSC [21, 22, 30, 63, 64]. As described in section 2, the HH also applies to harmonic molecules strongly coupled to a cavity mode. Thus, our work could hint at the observed resonant modification of reactions in polaritonic chemistry [30, 75, 76]. Notably, the beating period exhibits a sharp resonance in the strong coupling regime ($\lambda = 0.05$), while in the ultrastrong regime ($\lambda = 0.3$), the peak broadens as shown in figure 4(d). This is due to CRT, on which we focus next.

3.2. Effects of the counter-rotating terms on dynamical observables

The CRT make the polariton avoided crossing (figure 11) sensitive to the sign of the relative detuning, $\gamma - 1 = (\omega - \Omega)/\Omega$, and the difference between red- and blue-shifted cavity cases increases with λ (appendix B). This is a characteristic of the ultrastrong coupling regime [3, 4]. Consequently, the beating period, T is also sensitive to the detuning sign, as shown in figure 4(a). In contrast, under the rotating wave approximation (RWA), when the terms proportional to $\lambda \hat{a}^\dagger \hat{b}^\dagger$, $\lambda \hat{a}\hat{b}$ and λ^2 are omitted from equation (15)], $\bar{\Delta}_{\mathrm{RWA}} = \sqrt{(\gamma-1)^2 + \lambda^2}$ is independent of the detuning sign (appendix B). Figure 4(b) shows T_{RWA}, which remains the same for detunings of either sign.

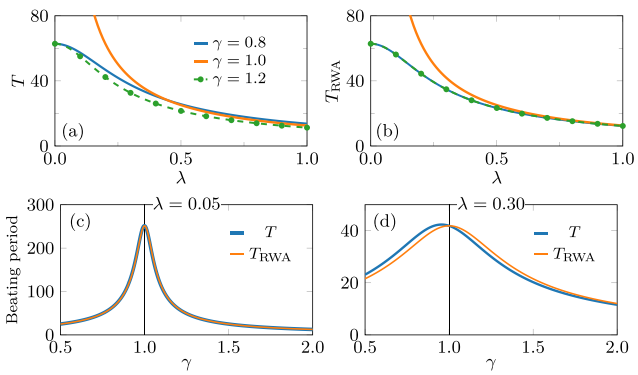

Figure 4. Dependence of the beating periods, $T \equiv 4\pi/(\Omega_+ - \Omega_-)$ (equation (17)) and $T_{\mathrm{RWA}} \equiv 4\pi/(\Omega_{\mathrm{RWA},+} - \Omega_{\mathrm{RWA},-})$ (equation (B2)) on (a), (b) λ and (c), (d) γ. T has a distinctive asymmetry as the cavity frequency is scanned through resonance. In contrast, T_{RWA} is independent of the sign of the detuning, such that the $\gamma = 0.8, 1.2$ curves in (b) overlap and the RWA curve in (d) is symmetric about the point $\gamma = 1$.

Figure 4(c) demonstrates that the RWA is a good approximation for $\lambda < 0.1$, as $T \approx T_{\mathrm{RWA}}$, which is expected. However, the asymmetry of T around $\gamma = 1$ becomes evident in panel (d). Additionally, the prefactor β in equation (20) vanishes at resonance under the RWA (appendix C). The asymmetries in the time-dependent matter CM quadrature are dynamic manifestations of the polariton branch asymmetry around $\gamma = 1$. Although the asymmetries of $\langle \hat{X}(t) \rangle$ arise from ultrastrong coupling, they are not inherently quantum effects. As mentioned earlier, in a system of coupled harmonic oscillators, the normal-mode frequencies, $\Omega_\pm$ and the first moments can be also determined by the classical solution, meaning similar features can be observed even in a pair of coupled classical oscillators. Therefore, next, we consider time-dependent observables defined in terms of the second moments of the light probability distribution to identify potential quantum effects. Figures 3(c) and (d) shows the evolution of the photon number expectation value, $\langle \hat{n}(t) \rangle$ at resonance ($\gamma = 1$). The local maxima correlate to when the phase space distribution is farthest from the origin (see figure 2). The beating period of $\langle \hat{n}(t) \rangle$ is given by $T/2$, since it includes the second moments, $\langle \hat{q}^2 \rangle$ and $\langle \hat{p}^2 \rangle$. More generally, observables involving higher moments of $\hat{X}$, $\hat{P}$ or $\hat{q}$, $\hat{p}$, i.e. $\langle \hat{X}^n \rangle$, $\langle \hat{P}^n \rangle$ or $\langle \hat{q}^n \rangle$, $\langle \hat{p}^n \rangle$ beat with period T for odd n and $T/2$ for even n. The time-averaged expectation value is given by (for the full expression, see appendix E)

$$\overline{\langle \hat{n} \rangle} \equiv \lim_{\tau \to \infty} \frac{1}{\tau} \int_0^\tau \langle \hat{n}(t) \rangle \, \mathrm{d}t \approx \Delta \overline{\langle \hat{n} \rangle} = \lambda^2 f_1 \left(w^{-2} - 1 \right) + \lambda^2 f_2 \left(2X_0^2 + w^2 - 1 \right), \tag{21}$$

where $\Delta \langle \hat{n}(t) \rangle \equiv \langle \hat{n}(t) \rangle - \langle \hat{n}(t; X_0 = 0, w = 1) \rangle$. To simplify the expression, we subtract the relatively small contribution from the average photon number when the CM is in the ground state. Here, $f_{1,2}$ are functions of γ and λ. At resonance, $\Delta \overline{\langle \hat{n}(\gamma = 1) \rangle} = X_0^2/4 + (w - w^{-1})^2/8$. For negligible matter squeezing ($w \approx 1$), $\Delta \overline{\langle \hat{n} \rangle} \approx (2\lambda^2 f_2) X_0^2$, and the average number of generated photons is determined by the initial CM shift, X_0. Figures 5(a) and (b) shows the dependence of $\Delta \overline{\langle \hat{n} \rangle}$ on λ and γ. The average photon number is asymmetric relative to the resonance point and fewer photons are generated, on average, for $\gamma > 1$. This asymmetry has important implications for the PND as well because, as we discuss next, the Q function is more negative in the blue-shifted cavity.

Under RWA, $\overline{\langle \hat{n} \rangle}_{\mathrm{RWA}} = \lambda^2 f_{\mathrm{RWA}} [2X_0^2 + (w - w^{-1})^2]$, and $f_{\mathrm{RWA}} = 1/[8(\gamma - 1)^2 + 8\lambda^2]$ is symmetric about $\gamma = 1$ (appendix E). Figures 5(c) and (d) shows the dependencies of $\overline{\langle \hat{n} \rangle}_{\mathrm{RWA}}$. In panel (c), the $\gamma = 0.8, 1.2$ and $\gamma = 0.9, 1.1$ curves overlap, while panel (d) demonstrates the symmetric Lorentzian function. The blue curves ($\lambda = 0.05$) in panels (b) and (d) are practically indistinguishable, suggesting that the RWA is a good approximation in the weak coupling regime ($\lambda \ll 1$).

The asymmetries in the time-averaged photon number reflect the effects of ultrastrong light-matter coupling. In contrast to the first moments, the photon number explicitly depends on the quantum uncertainty in position- and momentum-related quadratures. The average photon number is an experimentally accessible observable (for details, see section 5) and thus allows probing effects beyond RWA in quantum systems.

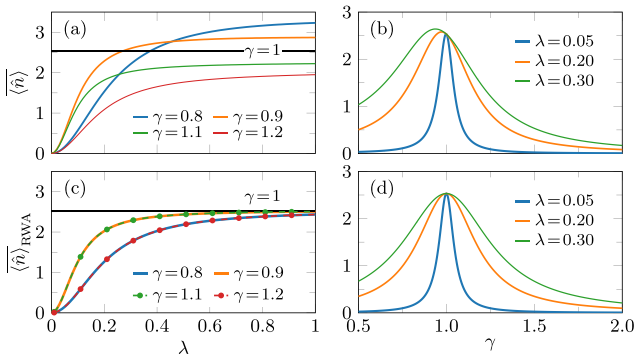

Figure 5. (a) and (b) Dependence of average photon number in equation (21) on λ and γ. (c) and (d) The same as in (a) and (b), but under RWA. At resonance, the average number of photons becomes independent of the coupling strength, λ in both the full system and under RWA–all graphs in panels (b) and (d) overlap at $\gamma = 1$. Note that in panel (d), the functions are symmetric Lorentzians centered at $\gamma = 1$.

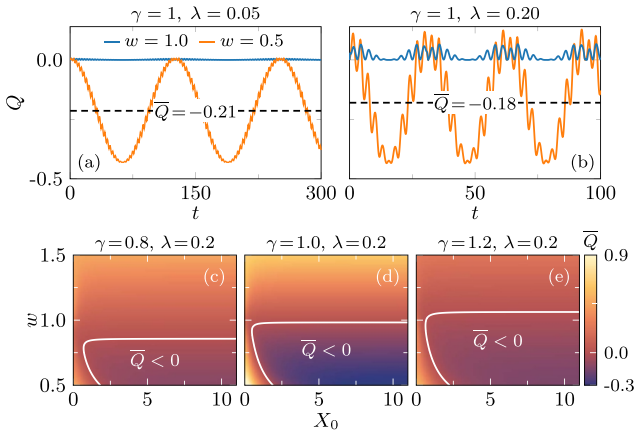

Figure 6. (a) and (b) Photon Mandel Q functions for the same parameters as in figures 3(c) and (d). Importantly, for $w = 0.5$, the time-averaged Q function, $\overline{Q}$ attains negative values. (c)–(e) The dependence of $\overline{Q}$ on the initial displacement and width of the matter CM state is shown before (c), at (d), and after (e) the resonance for strong cavity coupling. The nonclassical features of the photon state primarily occur for $w < 1$. At resonance in (d), the state transfer is most efficient. The asymmetry between (c) and (e) vanishes in the RWA (see appendix F), and $\overline{Q} < 0$ can be achieved only for $w < 1$.

3.3. Mandel Q function

Next, we focus on the Mandel Q function, which quantifies nonclassicality, indicated by negative values of Q. Figures 6(a) and (b) illustrates the evolution of the photon Q function at resonance. Q attains negative values only when CM is both shifted *and* quadrature-squeezed in X (i.e. when $w < 1$). Qualitatively, figure 2 suggests that the minimum of Q is connected to the initial value of Q_{mat}, given by $Q_{\mathrm{mat}}(0) = (w^2 - 1)[1 + \mathcal{O}(X_0^{-2})]$ (appendix F). While $\overline{\langle\hat{n}\rangle}$ in equation (21) scales with X_0^2, the initial Q_{mat} approaches a constant as X_0 increases, leading to the saturation of the minimal attainable Q values.

The time-averaged photon Mandel function, $\overline{Q} \equiv \lim_{\tau\to\infty} \tau^{-1} \int_0^\tau Q(t)\,\mathrm{d}t$, is shown in figures 6(c)–(e) for a range of X_0 and w values. $\overline{Q}$ is negative on either side of the resonance for an initially shifted and quadrature-squeezed matter state. Notably, Q may attain negative values for an initially quadrature-squeezed matter state even without the diamagnetic term ($\propto \lambda^2$) and under the RWA. However, under the RWA, the asymmetry between (c) and (e) disappears, and negative $\overline{Q}$ can be achieved only for $w < 1$ (appendix F).

It should be mentioned that internal quantum state transfer has previously been demonstrated in trapped atoms and ions in cavities [50, 51]. In these works, the cavity field interacts with the internal degree of freedom of a single atom or ion, such as a transition between two hyperfine or electronic states (two-level atoms). In contrast, our work explores coupling to a collective degree of freedom of many particles, e.g. the CM of harmonically trapped ions—a multilevel quantum system. Moreover, the coupling strength scales

with the particle number, N. This fundamental property enables reaching the ultrastrong light-matter coupling [3, 4], where the counter-rotating terms become important and introduce novel physical effects.

4. Scheme II. Generation of nonclassicality from a coherent cavity

An alternative approach for generating nonclassical states involves initializing the system with the matter CM in its ground state and the cavity in a coherent state, $|\alpha\rangle$. Figure 7 illustrates the evolution of the phase space distributions of matter CM (top row) and light (bottom row) in Scheme II. Initially, both Q and $Q_{\rm mat}$ are zero, as the system begins in a trivial state without any correlations. In this scenario, the counter-rotating interaction terms are crucial in generating sub-Poissonian distributions in the motional states of matter or photon number states (appendix F).

Over time, the matter and light distributions periodically elongate (squeeze); however, during maximal elongation, the matter phase space distribution aligns approximately along the line connecting its center to the origin, while the light distribution is oriented perpendicularly. As previously noted, the Q function becomes negative when the radial variance of the phase space distribution is less than the radial displacement. In this scenario, only the photon Q function attains negative values. In contrast to the resonance case shown in figure 2, the state transfer is only partial due to the large detuning. The matter phase space distribution does not reach the initial radial displacement of the light distribution, and the light distribution does not collapse to the origin.

Figure 8 shows the time averaged photon $\overline{Q}$ (top panels) and matter $\overline{Q}_{\rm mat}$ (bottom panels). $\overline{Q}$ is sensitive to the phase of α, negative $\overline{Q}$ is obtained before (after) the resonance for coherent states with sufficiently large Re$[\alpha]$ (Im$[\alpha]$). The Q functions reach saturation along the real or imaginary axes. At resonance, both $\overline{Q}$ and $\overline{Q}_{\rm mat}$ remain non-negative. Additionally, a clear asymmetry appears between the red and blue detuned cavities in panels (a) and (c). This asymmetry increases with λ, and, in the case of photons, culminates with the complete absence of $\overline{Q} < 0$ in the red-shifted cavity in the ultra-strong coupling regime ($\lambda = 0.5$, see appendix F).

Remarkably, under initial conditions where the photon $\overline{Q} \geqslant 0$ in figures 8(a) and (c), $\overline{Q}_{\rm mat}$ attains negative values. In other words, even when the sub-Poissonian PND is not achieved, the coherent state is partially transferred to the matter subsystem, simultaneously developing the sub-Poissonian distribution of motional states of the *matter* CM. The generation of nonclassical states in light and matter, starting from a coherent state of light, represents a key finding of this work.

The average number of photons, $\overline{\langle\hat{n}\rangle}$, is also sensitive to the phase of α and shows trends similar to those of $\overline{Q}$. The symmetries of $\overline{\langle\hat{n}\rangle}$ can be accessed via $\delta\overline{\langle\hat{n}\rangle} \equiv \overline{\langle\hat{n}(\alpha = C)\rangle} - \overline{\langle\hat{n}(\alpha = \mathrm{i}C)\rangle}$, where $C > 0$. $\delta\overline{\langle\hat{n}\rangle}$ measures the difference in average photon number between the initial coherent state with real α vs. imaginary α, and it is given by

$$\delta\overline{\langle\hat{n}\rangle} = \lambda^2 C^2 \frac{\left(2\gamma + \lambda^2\right)\left(\Omega_+^2 + \Omega_-^2\right) - 4\gamma}{4\bar{\Sigma}^2\bar{\Delta}^2}. \tag{22}$$

Figure 9 shows the dependence of $\delta\overline{\langle\hat{n}\rangle}/C^2$ on the system parameters. Here, the value of C is large enough to saturate the Q parameter. On average, the cavity is populated with fewer photons for real α (imaginary α), before (after) the resonance.

Moreover, the asymmetry of $|\delta\overline{\langle\hat{n}\rangle}|$ increases with λ. In the RWA, $\delta\overline{\langle\hat{n}\rangle} = 0$. To our knowledge, this asymmetry in photon generation as light-matter coupling enters the ultrastrong regime has not been previously discussed. This phenomenon could potentially be tested in Landau polariton systems, where ultrastrong coupling has been experimentally demonstrated [3, 4, 8, 12]. Such observation would provide clear evidence of the dynamical manifestation of ultrastrong coupling, extending our understanding of this regime beyond conventional spectroscopic methods.

Nonclassical states of light and matter have been extensively studied in optomechanical systems [35, 38]. However, the coupling mechanism in these systems differs from that considered here. In optomechanical systems, the cavity field interacts with the mechanical mode via polarizability. Additionally, achieving strong coupling requires external laser pumping near the cavity resonance. In contrast, in our case, the cavity field couples to charges in the matter subsystem, and the collective nature of the coupling allows us to reach the ultrastrong coupling regime and observe phenomena beyond the RWA described in this section.

5. How to access the nonclassical states

In Scheme I, the nonclassical photons generated in the cavity can be extracted by making one of the cavity mirrors semi-transparent [82, 105]. Photon leakage can modeled as coupling of the cavity field to a photonic

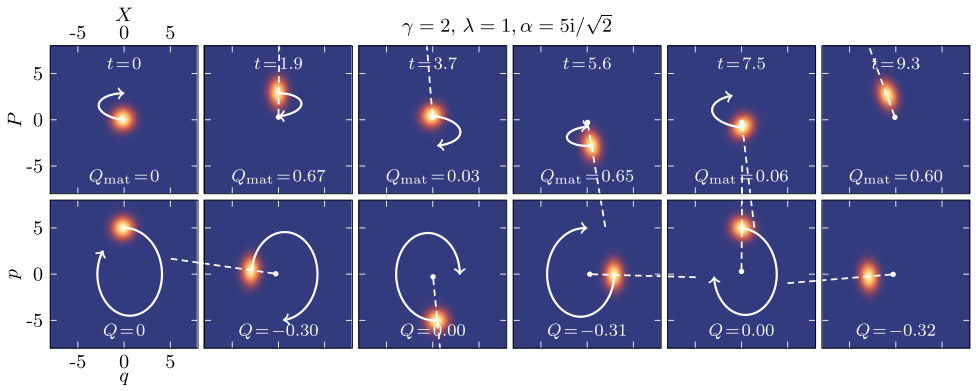

Figure 7. Snapshots of evolving phase space distribution of matter (X, P, upper row) and cavity field (q, p, bottom row). The initial state in Scheme II is a product of matter CM ground state and cavity coherent state, $|\alpha\rangle$. The arrows show the trajectories of the distribution centers. The dashed lines pass through the origin and distribution centers in each panel. Note that the matter distributions approximately align with the dashed lines, while the light distributions are perpendicular. The values of detuning and coupling constant are exaggerated to highlight the effect.

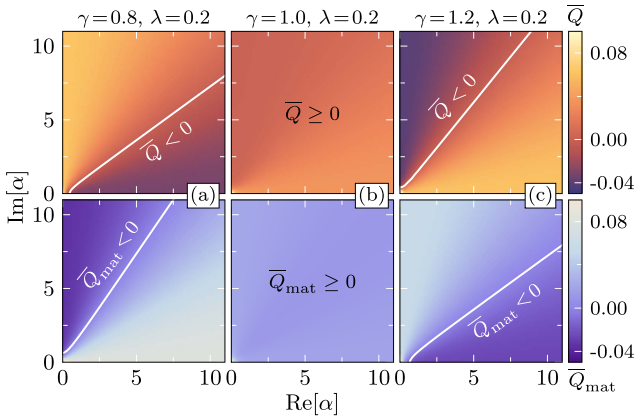

Figure 8. The dependence of photon $\overline{Q}$ (top panels) and the matter $\overline{Q}_{\rm mat}$ (bottom panels) on the initial coherent state, $|\alpha\rangle$. Sub-Poissonian distributions of photon and motional states are achieved off-resonance in (a) and (c). With increasing Re$[\alpha]$ and Im$[\alpha]$ components, the sub-Poissonian distributions saturate. At resonance, both photon and matter Mandel Q parameters are positive.

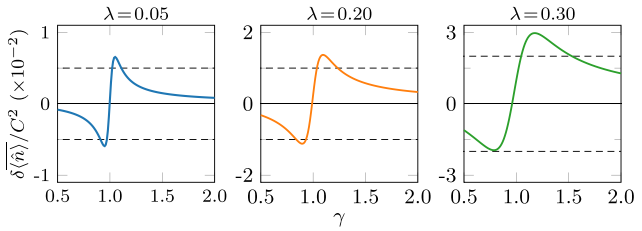

Figure 9. Dependence of $\delta\overline{\langle\hat{n}\rangle}/C^2$ in equation (22) on γ. In all cases, on average, the cavity is populated with more photons starting from a coherent state with imaginary (real) α below (above) resonance. The asymmetry of $|\delta\overline{\langle\hat{n}\rangle}|$ about $\gamma = 1$ increases with λ.

bath. The output field is obtained by employing the input-output formalism, which assumes a bilinear coupling to the bath degrees of freedom (cavity environment) through the field operators $\hat{a}$ and $\hat{a}^\dagger$, with a constant coupling proportional to $\sqrt{\kappa}$. In this framework, the equation of motion of the cavity field operator, $\hat{a}(t)$ includes damping terms, and depends on the input field operator, $\hat{d}_{\rm in}(t)$, which represents the

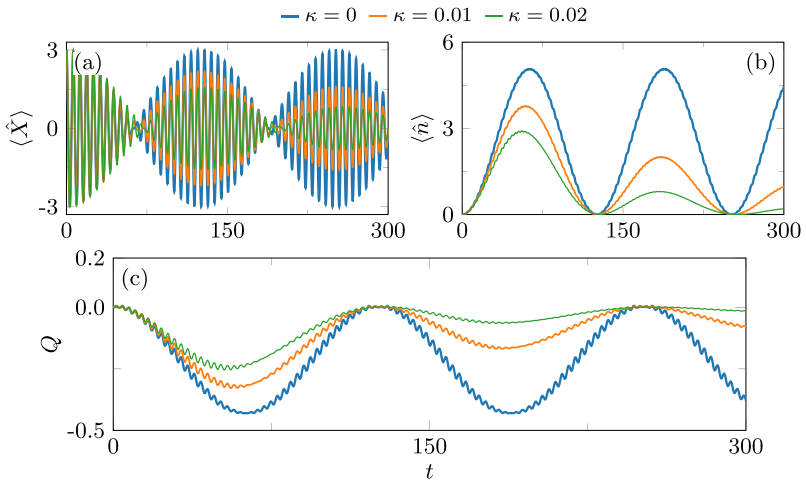

Figure 10. Expectation values of (a) matter CM X quadrature, (b) photon number, and (c) cavity photon Q function in the presence of cavity loss. The results were obtained by numerically solving equation (24). Parameters: $\gamma = 1$, $X_0 = 3$, $w = 0.5$.

environmental noise feeding into the cavity,

$$\dot{\hat{a}}(t) = -\mathrm{i}\left[\hat{a}(t), \hat{\mathcal{H}}\right] - \left[\hat{a}(t), \hat{a}^\dagger\right]\left(\frac{\kappa}{2}\hat{a} + \sqrt{\kappa}\hat{d}_{\mathrm{in}}(t)\right) + \left(\frac{\kappa}{2}a^\dagger + \sqrt{\kappa}\hat{d}_{\mathrm{in}}(t)\right)\left[\hat{a}(t), a\right]. \tag{23}$$

The cavity field operator, the input operator, and the output field operator, $\hat{d}_{\mathrm{out}}(t)$ are related via the input-output relation, $\hat{d}_{\mathrm{out}}(t) - \hat{d}_{\mathrm{in}}(t) = \sqrt{\kappa}\hat{a}(t)$ [106].

In practice, the effect of outcoupling can be modeled by the master equation for the reduced density matrix of the system, $\hat{\rho}$. This approach is valid under the assumption of weak coupling between the system and bath operators, as established in [106]. In the low-temperature limit ($k_B T \ll \hbar\omega_i$, where ω_i is an eigenfrequency of the system), the master equation becomes [106]

$$\dot{\hat{\rho}} = -\mathrm{i}\left[\hat{\mathcal{H}}, \hat{\rho}\right] + \frac{\kappa}{2}\left(2\hat{a}\hat{\rho}\hat{a}^\dagger - \hat{a}^\dagger\hat{a}\hat{\rho} - \hat{\rho}\hat{a}^\dagger\hat{a}\right). \tag{24}$$

Figure 10 shows expectation values, including the Q function of the cavity field, obtained by numerically solving equation (24). The observables exhibit persistent oscillations, exponentially decaying at an approximate rate of $\kappa/2$ (for the relatively small values of κ, $\kappa \ll \Omega$).

The expected number of photons leaking from the cavity can be roughly estimated by neglecting the input field in the input–output relation, $\hat{d}_{\mathrm{out}}(t) \approx \sqrt{\kappa}\hat{a}(t)$, such that $\langle\hat{n}_{\mathrm{out}}(t)\rangle \approx \kappa\langle\hat{n}(t)\rangle$, where $\hat{n}_{\mathrm{out}} \equiv \hat{d}^\dagger_{\mathrm{out}}\hat{d}_{\mathrm{out}}$. Then, the time-averaged expectation value of the photons outside the cavity is approximately given by $\overline{\langle\hat{n}_{\mathrm{out}}(t)\rangle} \approx \kappa\overline{\langle\hat{n}\rangle}\exp(-\kappa t/2)$ where $\overline{\langle\hat{n}\rangle}$ is the time-averaged number of photons in the isolated cavity in equation (21).

The Mandel Q function of the output field can be simply estimated using the following definition [102], $Q_{\mathrm{out}} = (\langle\hat{b}^\dagger_{\mathrm{out}}\hat{b}^\dagger_{\mathrm{out}}\hat{b}_{\mathrm{out}}\hat{b}_{\mathrm{out}}\rangle - \langle\hat{n}_{\mathrm{out}}\rangle^2)/\langle\hat{n}_{\mathrm{out}}\rangle = \kappa(\langle\hat{a}^\dagger\hat{a}^\dagger\hat{a}\hat{a}\rangle - \langle\hat{n}\rangle^2)/\langle\hat{n}\rangle = \kappa Q$. More rigorous treatment of the correlation functions involving $\hat{b}_{\mathrm{out}}$ is described in [106]. Constrained optimization can be employed to simultaneously minimize Q_{out} and maximize $\langle\hat{n}_{\mathrm{out}}\rangle$, thereby optimizing detection efficiency, but this is beyond the scope of the present study.

Alternatively, in Scheme II, the sub-Poissonian distribution of the matter CM states can be directly observed via spectroscopic methods, such as sideband spectroscopy for trapped atomic ions [49, 52]. Light and matter can be decoupled by introducing a large detuning to measure the properties of matter independently. The method and the details for introducing detuning will depend on the system and experimental setup. It is worth noting that in molecular polaritonics, the molecules are typically embedded in a solvent/matrix, which can be effectively treated as a separate bath for the molecules. The coupling to the solvent, however, under certain conditions, may become strong and drive non-trivial dynamics potentially affecting chemical reactions [77, 107]. This is outside the scope of this work and requires treatments beyond the weak system-bath interaction.

6. Conclusions and outlook

By leveraging the formation of polaritons in strongly and ultrastrongly coupled light-matter systems, we propose two initialization schemes to generate and effectively exchange nonclassical states of matter and light. In Scheme I, an initially displaced and quadrature-squeezed matter CM state is dynamically transferred to the cavity mode, producing nonclassical photons that can be extracted by making one of the cavity mirrors semi-transparent. This scheme builds upon the ability to create coherent and quadrature-squeezed matter states in ion traps (e.g. see [49]).

The second initialization scheme relies on ultrastrong coupling (i.e. on the presence of CRT in the Hamiltonian), which generates sub-Poissonian distributions of photon or matter states, starting from a coherent cavity state. This shows that an ultrastrongly coupled light-matter system acts as a generator that converts a coherent photonic state, devoid of nonclassical characteristics, into a nonclassical state of light or matter. This demonstrates a clear quantum advantage of the ultrastrong coupling regime [3, 4] and suggests novel pathways for hybrid, polaritonic quantum technologies. For example, one could envision protocols where matter is prepared in such a state that the system evolves into a macroscopic cat state [87] or a photonic cluster state [88], which can be used for quantum information and computation.

The population distribution of the matter states can be measured spectroscopically after decoupling the matter from the cavity. Additional manifestations of the ultrastrong coupling effects are the distinctive asymmetries in dynamical observables, such as average photon number and Mandel Q parameter, emerging as the cavity frequency is scanned through the resonance. These CRT-induced asymmetries provide a novel, dynamical perspective on the ultrastrong coupling regime typically probed by transmission spectroscopy. To our knowledge, such dynamic asymmetries have not been reported elsewhere.

The considered schemes can act as probes of quantum dynamics under strong or ultrastrong light-matter coupling in microscopic and mesoscopic systems. The coupling to light in such systems differs from that in typical optomechanical systems [35]. Initializing the cavity field in non-trivial states may enable new quantum control schemes for chemical processes in molecular systems under VSC. This could lead to applications in catalysis or the development of novel reaction pathways influenced by quantum states of light. Similarly, for Landau levels coupled to the cavity mode, strong light-matter interactions can transfer states of light to the electronic subsystem's collective (CM) mode, offering new ways to control electronic properties. Once a strong-ultrastrong coupling regime between the trapped ion's motion and the cavity mode is achieved, nonclassical photons could be potentially generated from squeezed motional states of ions. Nonclassical photonic states are important for quantum sensing [83–86].

We anticipate that our analysis will inspire further experimental and theoretical investigations of the dynamics in various strongly and ultrastrongly coupled light-matter systems, ultimately advancing the field of quantum science and technology and bridging it with polaritonic chemistry [22, 75, 76] and cavity quantum materials [16, 30].

Data availability statement

All data that support the findings of this study are included within the article (and any supplementary files).

Acknowledgments

IT, VR, and HRS acknowledge support from the NSF through a grant for ITAMP at Harvard University. IT was also supported by an NSF Subcontract No. 3357 at the Smithsonian Astrophysical Observatory. JC acknowledges support from the NSF (Grants Nos. CHE1800301 and CHE2324300), and the MIT Sloan Fund.

Appendix A. Mapping to the HH for different systems

In this appendix, we detail the intermediate steps involved in separating the Hamiltonians of the various systems in section 2 into the HH and a Hamiltonian describing the dynamics of the relative degrees of freedom.

A.1. Cold trapped ions

The collective coupling between the trapped ions and the cavity field emerges by transforming the Hamiltonian in equation (1) to the CM frame. We use a similar transformation for the other systems, too, later, so all the steps are detailed here. For mathematical convenience, we utilize a symmetric definition of the

collective and relative degrees of freedom, where both are scaled by $\sqrt{N}$ [90],

$$\hat{\mathbf{R}} = \frac{1}{\sqrt{N}}\sum_{i=1}^{N}\hat{\mathbf{r}}_i \quad \text{and} \quad \hat{\tilde{\mathbf{r}}}_j = \frac{\hat{\mathbf{r}}_1 - \hat{\mathbf{r}}_j}{\sqrt{N}} \quad \text{with} \quad j > 1. \tag{A1}$$

The momenta of the particles in the new coordinate system are given by $\nabla_1 = (\nabla_{\mathbf{R}} + \sum_{j=2}^{N}\widetilde{\nabla}_j)/\sqrt{N}$ and $\nabla_j = (\nabla_{\mathbf{R}} - \widetilde{\nabla}_j)/\sqrt{N}$, with $j > 1$. The kinetic energy terms in the new frame are given by

$$\sum_{i=1}^{N}\nabla_i^2 = \nabla_{\mathbf{R}}^2 + \frac{1}{N}\sum_{j=2}^{N}\widetilde{\nabla}_j^2 + \frac{1}{N}\sum_{j,k=2}^{N}\widetilde{\nabla}_j\cdot\widetilde{\nabla}_k. \tag{A2}$$

In the new coordinates, the cavity field couples only to the CM momentum, $\hat{\mathbf{A}}\cdot\sum_{i=1}^{N}\nabla_i = \sqrt{N}\hat{\mathbf{A}}\cdot\boldsymbol{\nabla}_{\mathbf{R}}$, while the scalar trapping potential separates into two parts, one depending on the CM coordinate and the other one on the relative coordinates, without cross-terms between the two

$$\sum_{i=1}^{N}\hat{\mathbf{r}}_i^2 = \hat{\mathbf{R}}^2 + N\sum_{j=2}^{N}\hat{\mathbf{r}}_j^2 - \left[\sum_{j=2}^{N}\hat{\mathbf{r}}_j\right]^2. \tag{A3}$$

The two-body interaction $W(\hat{\mathbf{r}}_i - \hat{\mathbf{r}}_l)$ depends only on the relative distances and thereby does not affect the cavity-induced CM motion. In the CM frame, it is given by

$$\sum_{i<l}^{N}W(\hat{\mathbf{r}}_i - \hat{\mathbf{r}}_l) = \sum_{1<l}^{N}W\left(\sqrt{N}\hat{\tilde{\mathbf{r}}}_l\right) + \sum_{2\leqslant i<l}^{N}W\left(\sqrt{N}\left(\hat{\tilde{\mathbf{r}}}_i - \hat{\tilde{\mathbf{r}}}_l\right)\right). \tag{A4}$$

The analysis above shows that the Hamiltonian separates into two parts, $\hat{H}_{\text{ion}} = \hat{H}_{\text{ion-cm}} + \hat{H}_{\text{ion-rel}}$, where (i) $\hat{H}_{\text{ion-cm}}$, describes the CM coupling to the quantized field $\hat{\mathbf{A}}$, and (ii) $\hat{H}_{\text{ion-rel}}$, describes the dynamics of the relative coordinates, decoupled from $\hat{\mathbf{A}}$ and the CM. The two parts are given by

$$\begin{aligned}
\hat{H}_{\text{ion-cm}} &= \frac{1}{2m}\left(\mathrm{i}\hbar\nabla_{\mathbf{R}} + g_0\sqrt{N}\hat{\mathbf{A}}\right)^2 + \frac{m\Omega^2}{2}\hat{\mathbf{R}}^2 + \sum_{\nu=x,y}\hbar\omega\left(\hat{a}_\nu^\dagger\hat{a}_\nu + \frac{1}{2}\right),\\
\hat{H}_{\text{ion-rel}} &= -\frac{\hbar^2}{2mN}\sum_{j=2}^{N}\widetilde{\nabla}_j^2 - \frac{\hbar^2}{2mN}\sum_{j,k=2}^{N}\widetilde{\nabla}_j\cdot\widetilde{\nabla}_k + \frac{mN\Omega^2}{2}\sum_{j=2}^{N}\hat{\tilde{\mathbf{r}}}_j^2\\
&\quad - \frac{m\Omega^2}{2}\left[\sum_{j=2}^{N}\hat{\tilde{\mathbf{r}}}_j\right]^2 + \sum_{1<l}^{N}W\left(\sqrt{N}\hat{\tilde{\mathbf{r}}}_l\right) + \sum_{2\leqslant i<l}^{N}W\left(\sqrt{N}\left(\hat{\tilde{\mathbf{r}}}_i - \hat{\tilde{\mathbf{r}}}_l\right)\right).
\end{aligned} \tag{A5}$$

In addition, it is crucial to demonstrate that the CM and relative degrees of freedom are independent by checking the commutation relations between their coordinates and momenta. Using the chain rule, we find the derivatives in the CM frame

$$\nabla_{\mathbf{R}} = \frac{1}{\sqrt{N}}\sum_{i=1}^{N}\nabla_i \quad \text{and} \quad \widetilde{\nabla}_j = \frac{1}{\sqrt{N}}\sum_{i=1}^{N}\nabla_i - \sqrt{N}\nabla_j \quad \text{with} \quad j > 1. \tag{A6}$$

It is clear that the momenta in the new frame of reference commute, $[\nabla_{\mathbf{R}}, \widetilde{\nabla}_j] = 0$. It can also be shown that the momenta and coordinates are independent since $[\nabla_{\mathbf{R}}, \hat{\tilde{\mathbf{r}}}_j] = 0$ and $[\widetilde{\nabla}_j, \hat{\mathbf{R}}] = 0$. Thus, we focus on the CM part to describe the cavity-matter dynamics. Since the polarization vectors of the photon field lie in the (x, y) plane, the z direction of the system becomes trivial. The light-matter Hamiltonian then describes a system of interacting harmonic oscillators, and importantly, the x and y directions are independent,

$$\hat{H}_{\text{ion-cm}} = \sum_{\nu=x,y}\left[-\frac{\hbar^2}{2m}\partial_{R_\nu}^2 + \frac{\mathrm{i}g_0\hbar}{m}\sqrt{N}\hat{A}_\nu\partial_{R_\nu} + \frac{m\Omega^2}{2}\hat{R}_\nu^2 + \frac{Ng_0^2}{2m}\hat{A}_\nu^2 + \hbar\omega\left(\hat{a}_\nu^\dagger\hat{a}_\nu + \frac{1}{2}\right)\right]. \tag{A7}$$

To avoid any confusion, note that $\hat{\mathbf{R}} = (\hat{R}_x, \hat{R}_y) = (\hat{X}, \hat{Y})$, $\nabla_{\mathbf{R}} = (\partial_{R_x}, \partial_{R_y}) = (\partial_X, \partial_Y)$ and $\hat{\mathbf{A}} = (\hat{A}_x, \hat{A}_y)$. Consequently, we can treat only one of the system's equivalent directions. Thus, the Hamiltonian that captures the ion-cavity dynamics is given by

$$\hat{H}_{\text{ion-cm}} = -\frac{\hbar^2}{2m}\partial_X^2 + \frac{m\Omega^2}{2}\hat{X}^2 + \frac{\mathrm{i}g_0\hbar}{m}\sqrt{N}\hat{A}_x\partial_X + \frac{Ng_0^2}{2m}\hat{A}_x^2 + \hbar\omega\left(\hat{a}_x^\dagger\hat{a}_x + \frac{1}{2}\right). \tag{A8}$$

Finally, in terms of the matter annihilation operators

$$\hat{b}_x = \sqrt{\frac{m\Omega}{2\hbar}}\left(\hat{X} + \frac{\hbar}{m\Omega}\partial_X\right), \tag{A9}$$

the CM Hamiltonian attains the form of the well-known HH [3, 41]

$$\hat{H}_{\text{ion-cm}} = \hbar\Omega\left(\hat{b}_x^\dagger\hat{b}_x + \frac{1}{2}\right) - \mathrm{i}\sqrt{\frac{\hbar\Omega g_0^2 N}{2m}}\hat{A}_x\left(\hat{b}_x^\dagger - \hat{b}_x\right) + \frac{Ng_0^2}{2m}\hat{A}_x^2 + \hbar\omega\left(\hat{a}_x^\dagger\hat{a}_x + \frac{1}{2}\right). \tag{A10}$$

A.2. Landau levels

This subsection details the transformation of the 2deg Hamiltonian, $\hat{H}_{\text{2deg}}$ in equation (6). The interaction term between the cavity field and the dynamical momenta of electrons is given by

$$\hat{\mathbf{A}}\cdot\sum_{i=1}^{N}\mathrm{i}\hbar\nabla_i + e\mathbf{A}_{\text{ext}}\left(\hat{\mathbf{r}}_i\right) = \sqrt{N}\hat{\mathbf{A}}\cdot\left[\mathrm{i}\hbar\nabla_{\mathbf{R}} + e\mathbf{A}_{\text{ext}}\left(\hat{\mathbf{R}}\right)\right]. \tag{A11}$$

In terms of the new coordinates, the sum of squares of the external field is

$$\sum_{i=1}^{N}\mathbf{A}_{\text{ext}}^2\left(\hat{\mathbf{r}}_i\right) = \mathbf{A}_{\text{ext}}^2\left(\hat{\mathbf{R}}\right) + N\sum_{j=2}^{N}\mathbf{A}_{\text{ext}}^2\left(\hat{\tilde{\mathbf{r}}}_j\right) - \left[\sum_{j=2}^{N}\mathbf{A}_{\text{ext}}\left(\hat{\tilde{\mathbf{r}}}_j\right)\right]^2. \tag{A12}$$

The bilinear term involving the magnetic field and momenta is given by

$$\sum_{i=1}^{N}\mathbf{A}_{\text{ext}}\left(\hat{\mathbf{r}}_i\right)\cdot\nabla_i = \mathbf{A}_{\text{ext}}\left(\hat{\mathbf{R}}\right)\cdot\nabla_{\mathbf{R}} + \sum_{j=2}^{N}\mathbf{A}_{\text{ext}}\left(\hat{\tilde{\mathbf{r}}}_j\right)\cdot\tilde{\nabla}_j. \tag{A13}$$

Collecting the terms, we find that the Hamiltonian in the new frame is a sum of two terms, $\hat{H}_{\text{2deg}} = \hat{H}_{\text{2deg-cm}} + \hat{H}_{\text{2deg-rel}}$, where: (i) the CM term, $\hat{H}_{\text{2deg-cm}}$ including the coupling to the quantized field $\hat{\mathbf{A}}$, and (ii) the term $\hat{H}_{\text{2deg-rel}}$ depending on the relative distances, decoupled from $\hat{\mathbf{A}}$. The two terms are given by

$$\begin{aligned}
\hat{H}_{\text{2deg-cm}} &= \frac{1}{2m}\left(\mathrm{i}\hbar\nabla_{\mathbf{R}} + e\mathbf{A}_{\text{ext}}\left(\hat{\mathbf{R}}\right) + e\sqrt{N}\hat{\mathbf{A}}\right)^2 + \hbar\omega\left(\hat{a}^\dagger\hat{a} + \frac{1}{2}\right),\\
\hat{H}_{\text{2deg-rel}} &= \frac{1}{2m}\sum_{j=2}^{N}\left[\frac{\mathrm{i}\hbar\tilde{\nabla}_j}{\sqrt{N}} + e\sqrt{N}\mathbf{A}_{\text{ext}}\left(\hat{\tilde{\mathbf{r}}}_j\right)\right]^2 - \frac{\hbar^2}{2mN}\sum_{j,l=2}^{N}\tilde{\nabla}_j\cdot\tilde{\nabla}_l - \frac{e^2}{2m}\left[\sum_{j=2}^{N}\mathbf{A}_{\text{ext}}\left(\hat{\tilde{\mathbf{r}}}_j\right)\right]^2\\
&\quad + \sum_{1<l}^{N}W\left(\sqrt{N}\hat{\tilde{\mathbf{r}}}_l\right) + \sum_{2\leqslant i<l}^{N}W\left(\sqrt{N}\left(\hat{\tilde{\mathbf{r}}}_i - \hat{\tilde{\mathbf{r}}}_l\right)\right).
\end{aligned} \tag{A14}$$

Appendix B. Polariton branches

This appendix presents the polariton frequencies and their dependence on the collective coupling constant, λ and $\gamma \equiv \omega/\Omega$. Here, ω is the cavity mode frequency, and Ω is the harmonic matter trap frequency. The dimensionless upper/lower polariton frequencies are defined in equation (17) [40],

$$\Omega_\pm^2 = \frac{1+\gamma^2+\gamma\lambda^2}{2} \pm \frac{1}{2}\sqrt{\left(1+\gamma^2+\gamma\lambda^2\right)^2 - 4\gamma^2}, \tag{B1}$$

where the collective coupling constant depends on the number of trapped particles, $N \geqslant 1$ as $\lambda \equiv \sqrt{2Ng_0^2/(\pi\epsilon_0 c\mathcal{A}m\Omega)}$. Here, g_0 is the single particle coupling constant, $\mathcal{A}$ is the area of the resonator mirror, m is the particle mass, ϵ_0 is the vacuum permittivity, c is the speed of light.

Figure 11 shows the λ,γ-dependence of $\Omega_\pm$ and VRS, $\tilde{\Delta} \equiv (\Omega_+ - \Omega_-) = \sqrt{(1-\gamma)^2+\gamma\lambda^2}$. Note that the asymmetry relative to the point $\gamma = 1$ increases with λ. Under the RWA, the terms proportional to $\lambda\hat{a}^\dagger\hat{b}^\dagger, \lambda\hat{a}\hat{b}$, and λ^2 in the Hamiltonian (see equation (15)) are omitted, and the polariton branches become

$$\Omega_{\text{RWA},\pm}^2 = \frac{1+\gamma^2+\lambda^2/2}{2} \pm \frac{1}{2}\sqrt{(\gamma+1)^2\left[(\gamma-1)^2+\lambda^2\right]}. \tag{B2}$$

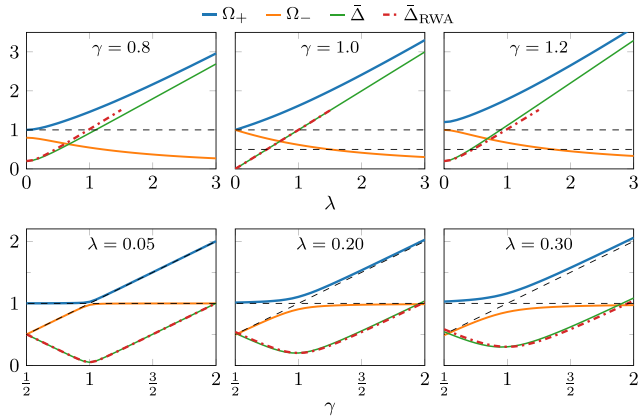

Figure 11. Top panels—Polariton branches, $\Omega_\pm$ and VRS, $\bar{\Delta} \equiv \Omega_+ - \Omega_-$ and $\bar{\Delta}_{\mathrm{RWA}} \equiv \Omega_{\mathrm{RWA},+} - \Omega_{\mathrm{RWA},-}$, as a function of the collective coupling constant, λ. At resonance ($\gamma = 1$), $\bar{\Delta} = \bar{\Delta}_{\mathrm{RWA}} = \lambda$. The difference between $\bar{\Delta}$ and $\bar{\Delta}_{\mathrm{RWA}}$ grows with λ. Bottom panels—$\Omega_\pm$, $\bar{\Delta}$, and $\bar{\Delta}_{\mathrm{RWA}}$ as a function of γ. $\bar{\Delta}$ develops asymmetry about $\gamma = 1$ with increasing λ, while $\bar{\Delta}_{\mathrm{RWA}} = \sqrt{(\gamma-1)^2 + \lambda^2}$ remains symmetric.

Under the RWA, the VRS, $\bar{\Delta}_{\mathrm{RWA}} = \Omega_{\mathrm{RWA},+} - \Omega_{\mathrm{RWA},-}$, is symmetric relative to $\gamma = 1$ and it is given by

$$\bar{\Delta}_{\mathrm{RWA}} = \sqrt{(\gamma-1)^2 + \lambda^2}. \tag{B3}$$

Appendix C. Semiclassical approach

The semiclassical approach relies on solving Hamilton's equations of motion derived from the classical counterpart of $\hat{\mathcal{H}}$ in equation (15)

$$\dot{X} = P - \lambda q, \quad \dot{P} = -X, \tag{C1a}$$
$$\dot{q} = \gamma p, \quad \dot{p} = -\gamma q + \lambda P - \lambda^2 q. \tag{C1b}$$

This system of linear differential equations can be solved by the Laplace transform method. Laplace transform, denoted by $\mathcal{L}$, turns the set of differential equations into a system of algebraic equations since $\mathcal{L}(\dot{f}) = \tilde{f}(s) - f(0)$, where $\tilde{f}(s)$ is the Laplace transform of f, s is the Laplace space variable, and $f(0)$ is the initial value of f. Solving the algebraic system yields,

$$\tilde{X}(s) = \frac{X(0)\left[s^3 + \gamma\left(\gamma+\lambda^2\right)s\right] + P(0)\left[s^2+\gamma^2\right]}{h(s)} - \lambda s \frac{q(0)s + \gamma p(0)}{h(s)}, \tag{C2a}$$
$$\tilde{P}(s) = \frac{\left[sP(0) - X(0)\right]\left[s^2 + \gamma\left(\gamma+\lambda^2\right)\right]}{h(s)} + \lambda \frac{q(0)s + \gamma p(0)}{h(s)}, \tag{C2b}$$
$$\tilde{q}(s) = \gamma\lambda s \frac{P(0) - X(0)}{h(s)} + \left(s^2+1\right)\frac{q(0)s + \gamma p(0)}{h(s)}, \tag{C2c}$$
$$\tilde{p}(s) = \lambda s \frac{P(0)s - X(0)}{h(s)} - \frac{q(0)\left[\gamma + s^2\left(\gamma+\lambda^2\right)\right]}{h(s)} + \frac{p(0)\left(s^3+s\right)}{h(s)}, \tag{C2d}$$

where $h(s) = s^4 + s^2[\gamma(\gamma+\lambda^2)+1] + \gamma^2$ is the characteristic polynomial of the linear system, and $X(0)$, $P(0)$, $q(0)$, and $p(0)$ are the initial values. The roots of $h(s)$ are given by $s_{1,2} = \mathrm{i}\Omega_\pm$ and $s_{3,4} = -\mathrm{i}\Omega_\pm$, where $\Omega_\pm$ are the upper/lower polariton frequencies in equation (B1). With those roots, $X(t)$, $P(t)$, $q(t)$ and $p(t)$ can be found by applying the inverse Laplace transform, $\mathcal{L}^{-1}$ to equations (C2a)–(C2d). The expectation values are obtained semiclassically by averaging the classical expression for an observable $\hat{O}(t)$, $O(t) = f[X(t), P(t), q(t), p(t)]$ with respect to the initial phase space distribution $\mathcal{P}(0)$

$$\langle \hat{O}(t) \rangle = \int \cdots \int_{-\infty}^{\infty} O(t)\,\mathcal{P}(0)\,\mathrm{d}\mathbb{V}, \tag{C3}$$

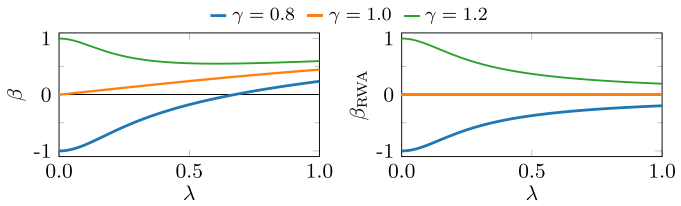

Figure 12. Factors β and β_{RWA} in equations (C5) and (C6). At resonance, β_{RWA} vanishes, while β scales approximately linearly with λ (for $\lambda < 1$). Moreover, $|\beta|$ is sensitive to the sign of the relative detuning, $\gamma - 1$, while $|\beta_{\mathrm{RWA}}|$ is not.

where $\mathrm{d}\mathbb{V} \equiv \mathrm{d}X(0)\mathrm{d}P(0)\mathrm{d}q(0)dp(0)$. The phase space distribution is derived from the initial wave function and thus accounts for the position-momentum uncertainty. For example, the wave function, $\psi_0(X,q) \propto \exp[-(X-X_0)^2/(2w^2)]\exp(-q^2/2)$ corresponds to the phase space distribution

$$\mathcal{P}(0) = \frac{1}{\pi^2}\exp\left[-\frac{(X(0)-X_0)^2}{w^2} - w^2P^2(0)\right]\exp\left[-q^2(0)-p^2(0)\right], \tag{C4}$$

where X_0 is the initial displacement of the matter CM quadrature and w is the initial width of the state (for the decoupled CM ground state, $w = 1$).

C.1. Expectation value of the matter CM X quadrature

In the case of $\langle\hat{X}(t)\rangle$, only the first term $\propto X(0)$ (see equation (C2*a*)) contributes to $X(t)$ after the integration in equation (C3). Simplification yields (same as equation (20))

$$\frac{\langle\hat{X}(t)\rangle}{X_0} = \cos\left[\frac{\bar{\Sigma}t}{2}\right]\cos\left[\frac{\bar{\Delta}t}{2}\right] + \beta\sin\left[\frac{\bar{\Sigma}t}{2}\right]\sin\left[\frac{\bar{\Delta}t}{2}\right], \tag{C5}$$

where $\bar{\Sigma} \equiv \Omega_+ + \Omega_-$, $\bar{\Delta} \equiv \Omega_+ - \Omega_- = \sqrt{(1-\gamma)^2+\gamma\lambda^2}$ is the VRS ($\bar{\Sigma} < \bar{\Delta}$), and $\beta = (\Omega_+^2 + \Omega_-^2 - 2)/(\bar{\Sigma}\bar{\Delta})$. Under RWA,

$$\frac{\langle\hat{X}(t)\rangle_{\mathrm{RWA}}}{X_0} = \cos\left[\frac{\bar{\Sigma}_{\mathrm{RWA}}t}{2}\right]\cos\left[\frac{\bar{\Delta}_{\mathrm{RWA}}t}{2}\right] + \beta_{\mathrm{RWA}}\sin\left[\frac{\bar{\Sigma}_{\mathrm{RWA}}t}{2}\right]\sin\left[\frac{\bar{\Delta}_{\mathrm{RWA}}t}{2}\right], \tag{C6}$$

where $\bar{\Sigma}_{\mathrm{RWA}}$, $\bar{\Delta}_{\mathrm{RWA}}$, β_{RWA} are defined in terms of $\Omega_{\mathrm{RWA},\pm}$, and $\bar{\Delta}_{\mathrm{RWA}} = \sqrt{(\gamma-1)^2+\lambda^2}$.

β factor.—Figure 12 compares β and β_{RWA}. At resonance, β scales approximately linearly with λ (for $\lambda < 1$), while $\beta_{\mathrm{RWA}}(\gamma = 1)$ vanishes. This suggests that the ultra-strong coupling effects in $\langle X(t)\rangle$, induced by CRT, are most emphasized at resonance.

Appendix D. Probability density and phase space distribution

In this appendix, we outline the semiclassical derivation of the exact matter CM probability density, $\mathcal{P}(X,t)$, and discuss its behavior in Scheme I (for shifted and squeezed matter initial state). Additionally, we present the general form of the matter and light phase space distributions.

To derive $\mathcal{P}(X,t)$, we first invert $X[t;X(0)]$ to obtain $X(0)$ as a function of time and the rest of the initial conditions

$$X(0) = \frac{X(t) - f_2(t)P(0) - f_3(t)q(0) - f_4(t)p(0)}{f_1(t)}. \tag{D1}$$

The functions, $f_{1,\ldots,4}(t)$ are given by

$$f_1(t) = \langle\hat{X}(t)\rangle/X_0, \tag{D2a}$$

$$f_2(t) = \frac{(\Omega_+^2-\gamma^2)\sin(\Omega_+t)}{\Omega_+\bar{\Delta}\bar{\Sigma}} - \frac{(\Omega_-^2-\gamma^2)\sin(\Omega_-t)}{\Omega_-\bar{\Delta}\bar{\Sigma}}, \tag{D2b}$$

$$f_3(t) = -\lambda\frac{\Omega_+\sin(\Omega_+t) - \Omega_-\sin(\Omega_-t)}{\bar{\Delta}\bar{\Sigma}}, \tag{D2c}$$

$$f_4(t) = \lambda\gamma\frac{\cos(\Omega_+t) - \cos(\Omega_-t)}{\bar{\Delta}\bar{\Sigma}}. \tag{D2d}$$

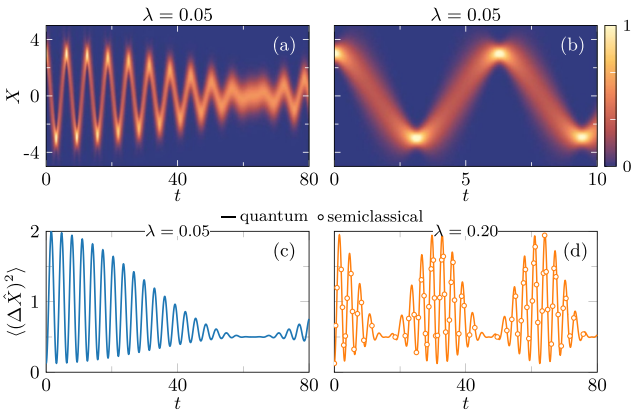

Figure 13. (a) and (b) Matter CM quadrature probability density, $\mathcal{P}(X,t)$ in equation (D5). The wave packet motion combines oscillations and breathing about the mean value. The total probability is conversed, which causes the bright spots when the width of the wave packet is minimized. (c) and (d) Variance of $\mathcal{P}(X,t)$. Local minima are attained at the turning points of the wave packet, i.e. at the extrema of $\langle\hat{X}(t)\rangle$). Parameters: $\gamma = 1$, $X_0 = 3$, $w = 0.5$.

Substituting the expression for $X(0)$ in equation (D1) into the initial phase space distribution in equation (C4) and integrating out $P(0)$, $q(0)$, and $p(0)$, yields

$$\mathcal{P}(X,t) = \frac{1}{\sqrt{\pi}\sqrt{w^2 f_1^2 + f_2^2/w^2 + f_3^2 + f_4^2}} \exp\left[-\frac{(X - f_1 X_0)^2}{w^2 f_1^2 + f_2^2/w^2 + f_3^2 + f_4^2}\right]. \tag{D3}$$

It can be shown that

$$w^2 f_1^2(t) + f_2^2(t)/w^2 + f_3^2(t) + f_4^2(t) = 2\langle\left[\Delta\hat{X}(t)\right]^2\rangle, \tag{D4}$$

where $\langle[\Delta\hat{X}(t)]^2\rangle \equiv \langle\hat{X}^2(t)\rangle - \langle\hat{X}(t)\rangle^2$. Thus,

$$\mathcal{P}(X,t) = \frac{1}{\sqrt{2\pi\langle\left[\Delta\hat{X}(t)\right]^2\rangle}} \exp\left[-\frac{\left(X - \langle\hat{X}(t)\rangle\right)^2}{2\langle\left[\Delta\hat{X}(t)\right]^2\rangle}\right]. \tag{D5}$$

Figures 13(a) and (b) shows an example of $\mathcal{P}(X,t)$. The CM wave packet combines oscillatory and breathing motions about the mean. The wave packet width (variance) increases between the turning points, as seen in figure 13(b). The bright spots in the density plots appear when the width is minimum, since the amplitude is maximized at those moments to conserve the total probability.

Phase space distributions.—Generally, phase space distributions of both matter and light subsystems are multivariate (2D) Gaussians. A Gaussian function in two dimensions (X and P, or q and p) is defined by five parameters, the coordinates of the center $[\mu_{X,P}(t)$ or $\mu_{q,p}(t)]$, and the elements of the symmetric covariance matrix

$$\mathbf{\Sigma}(t) = \begin{bmatrix} \sigma_X^2(t) & \sigma_{XP}(t) \\ \sigma_{XP}(t) & \sigma_P^2(t) \end{bmatrix} \quad \text{or} \quad \mathbf{\Sigma}(t) = \begin{bmatrix} \sigma_q^2(t) & \sigma_{qp}(t) \\ \sigma_{qp}(t) & \sigma_p^2(t) \end{bmatrix}. \tag{D6}$$

For example, the photon phase space distribution is given by

$$\mathcal{P}(q,p,t) = \frac{1}{2\pi\sqrt{\sigma_q^2\sigma_p^2 - \sigma_{qp}^2}} \exp\left[-\frac{\sigma_p^2\left(q-\mu_q\right)^2}{2\left(\sigma_q^2\sigma_p^2 - \sigma_{qp}^2\right)}\right] \exp\left[-\frac{\sigma_q^2\left(p-\mu_p\right)^2}{2\left(\sigma_q^2\sigma_p^2 - \sigma_{qp}^2\right)} + \frac{2\sigma_{qp}\left(q-\mu_q\right)\left(p-\mu_p\right)}{2\left(\sigma_q^2\sigma_p^2 - \sigma_{qp}^2\right)}\right], \tag{D7}$$

where $\sigma_\nu^2 \equiv \langle(\Delta\hat{\nu})^2\rangle = \langle\hat{\nu}^2\rangle - \mu_\nu^2$, $\sigma_{qp} \equiv \langle(\Delta\hat{q}\hat{p})\rangle = \langle\hat{q}\hat{p}\rangle - \mu_q\mu_p$, and $\mu_\nu \equiv \langle\hat{\nu}\rangle$ ($\nu = q,p$). Phase space distribution such as in equation (D7) appear as rotated ellipses centered around (μ_q,μ_p). The eigenvectors of the covariance matrix define the orientation of the ellipses, while the aspect ratio is proportional to the ratio of the eigenvalues.

Higher-order expectation values related to the matter or light subsystems can be conveniently obtained by averaging the corresponding classical expressions with respect to the phase space distributions. The higher-order averages over a 2D Gaussian distribution are entirely determined by the distribution's first two moments, namely the means (e.g. $\mu_{X,P}(t)$ or $\mu_{q,p}(t)$) and the elements of $\mathbf{\Sigma}$.

Appendix E. Photon number expectation value

In this appendix, we explore the properties of the photon number expectation value in Scheme I. We also consider the RWA, allowing us to isolate the ultrastrong-coupling effects arising from the counter-rotating and diamagnetic terms of the Hamiltonian.

E.1. Scheme I

Using the phase space distribution in equation (D7) the expectation value of the photon number $\hat{n} = \hat{a}^\dagger\hat{a} = (\hat{q}^2 + \hat{p}^2)/2 - 1/2$ can be conveniently found by following the semiclassical approach outlined in appendix C. To simplify the expression, we subtract the relatively small average photon number when the CM is in the ground state. Thus, the considered quantity is $\Delta\langle\hat{n}(t)\rangle \equiv \langle\hat{n}(t)\rangle - \langle\hat{n}(t; X_0 = 0, w = 1)\rangle$, which is given by

$$\begin{aligned}
&\Delta\langle\hat{n}(t)\rangle \\
&= \lambda^2\left(w^{-2}-1\right)\left(\gamma^2\frac{\sin^2\left(\bar{\Sigma}t/2\right)\sin^2\left(\bar{\Delta}t/2\right)}{\bar{\Sigma}^2\bar{\Delta}^2} + \frac{\left[\Omega_+\sin\left(\bar{\Sigma}t/2\right)\cos\left(\bar{\Delta}t/2\right) - \left(\bar{\Sigma}/2\right)\sin\left(\Omega_- t\right)\right]^2}{\bar{\Sigma}^2\bar{\Delta}^2}\right) \\
&\quad + \lambda^2\left(2X_0^2 + w^2 - 1\right)\left(\gamma^2\frac{\left[\Omega_-\sin\left(\bar{\Sigma}t/2\right)\cos\left(\bar{\Delta}t/2\right) - \left(\bar{\Sigma}/2\right)\sin\left(\Omega_- t\right)\right]^2}{\Omega_+^2\Omega_-^2\bar{\Sigma}^2\bar{\Delta}^2} + \frac{\sin^2\left(\bar{\Sigma}t/2\right)\sin^2\left(\bar{\Delta}t/2\right)}{\bar{\Sigma}^2\bar{\Delta}^2}\right),
\end{aligned} \tag{E1}$$

The time-averaged value reads

$$\Delta\overline{\langle\hat{n}\rangle} = \lambda^2\left(w^{-2}-1\right)f_1 + \lambda^2\left(2X_0^2 + w^2 - 1\right)f_2, \tag{E2}$$

where $f_{1,2}$ (see equation (21)) are defined as

$$f_1 = \frac{\Omega_+^2 + \Omega_-^2 + 2\gamma^2}{8\bar{\Sigma}^2\bar{\Delta}^2} = \frac{1}{8}\frac{\gamma\left(3\gamma+\lambda^2\right)+1}{\gamma^2\left[\left(\gamma+\lambda^2\right)^2 - 2\right] + 2\gamma\lambda^2 + 1}, \tag{E3a}$$

$$f_2 = \frac{2\Omega_+^2\Omega_-^2 + \gamma^2\left(\Omega_+^2 + \Omega_-^2\right)}{8\Omega_+^2\Omega_-^2\bar{\Sigma}^2\bar{\Delta}^2} = \frac{1}{8}\frac{\gamma\left(\gamma+\lambda^2\right)+3}{\gamma^2\left[\left(\gamma+\lambda^2\right)^2 - 2\right] + 2\gamma\lambda^2 + 1}. \tag{E3b}$$

At resonance, $f_{1,2}$ simplify to $f_1 = f_2 = 1/(8\lambda^2)$,and $\Delta\overline{\langle\hat{n}\rangle}$ becomes independent of λ,

$$\Delta\overline{\langle\hat{n}(\gamma=1)\rangle} = \frac{X_0^2}{4} + \frac{1}{8}\left(w - w^{-1}\right)^2. \tag{E4}$$

When $w \sim 1$, $\Delta\overline{\langle\hat{n}\rangle}$ can be roughly estimated by the single term proportional to X_0^2,

$$\Delta\overline{\langle\hat{n}\rangle} \approx 2\lambda^2 f_2 X_0^2. \tag{E5}$$

Figures 5(a) and (b) shows $\Delta\overline{\langle\hat{n}\rangle}$ as a function of λ and γ. In panel (b), the asymmetry about the point of resonance, $\gamma = 1$ increases with λ. Next, by comparison with the RWA, we demonstrate that the asymmetry stems from the ultrastrong coupling and CRT.

RWA.—In the RWA, the Hamiltonian takes the form

$$\hat{\mathcal{H}}_{\mathrm{RWA}} = \left[\hat{b}^\dagger\hat{b} + \frac{1}{2}\right] + \gamma\left[\hat{a}^\dagger\hat{a} + \frac{1}{2}\right] - \mathrm{i}\frac{\lambda}{2}\hat{b}^\dagger\hat{a} + \mathrm{i}\frac{\lambda}{2}\hat{b}\hat{a}^\dagger. \tag{E6}$$

Expressing $\hat{\mathcal{H}}_{\mathrm{RWA}}$ in terms of $\hat{X}$, $\hat{P}$, $\hat{q}$, and $\hat{p}$, and following the semiclassical approach, we can obtain the photon number expectation value

$$\begin{aligned}\langle \hat{n}(t)\rangle_{\mathrm{RWA}} &= \lambda^2\left[2X_0^2+\left(w-w^{-1}\right)^2\right]\frac{(\gamma+1)^2\sin^2\left(\bar{\Sigma}_{\mathrm{RWA}}t/2\right)\sin^2\left(\bar{\Delta}_{\mathrm{RWA}}t/2\right)}{4\bar{\Sigma}^2_{\mathrm{RWA}}\bar{\Delta}^2_{\mathrm{RWA}}}+\lambda^2\left[2X_0^2+\left(w-w^{-1}\right)^2\right]\\ &\times\frac{\left[\Omega_{\mathrm{RWA},-}\left(\gamma-\lambda^2/4+\Omega^2_{\mathrm{RWA},+}\right)\sin\left(\Omega_{\mathrm{RWA},+}t\right)-\Omega_{\mathrm{RWA},+}\left(\gamma-\lambda^2/4+\Omega^2_{\mathrm{RWA},-}\right)\sin\left(\Omega_{\mathrm{RWA},-}t\right)\right]^2}{16\Omega^2_{\mathrm{RWA},+}\Omega^2_{\mathrm{RWA},-}\bar{\Sigma}^2_{\mathrm{RWA}}\bar{\Delta}^2_{\mathrm{RWA}}},\end{aligned} \tag{E7}$$

where $\Omega_{\mathrm{RWA},\pm}$ are defined in equation (B2). Note that in the full system, $\overline{\langle\hat{n}\rangle}$ differs from zero for the CM ground state ($X_0=0$, $w=1$). That is why we defined $\Delta\langle\hat{n}(t)\rangle$ in equation (E1) to simplify the analysis. In contrast, under RWA, $\langle\hat{n}(t;X_0=0,w=1)\rangle\equiv 0$ as seen from equation (E7). The time average of $\langle\hat{n}(t)\rangle_{\mathrm{RWA}}$ is given by the simple expression

$$\overline{\langle\hat{n}\rangle}_{\mathrm{RWA}}=\frac{1}{8}\frac{\lambda^2}{(\gamma-1)^2+\lambda^2}\left[2X_0^2+\left(w-w^{-1}\right)^2\right]. \tag{E8}$$

At resonance ($\gamma=1$), $\overline{\langle\hat{n}\rangle}_{\mathrm{RWA}}$ reduces to equation (E4). Under RWA, the prefactor of X_0^2 (in this case, it is the overall prefactor) is a Lorentzian function of γ of width λ centered at $\gamma=1$,

$$2\lambda^2 f_{\mathrm{RWA}}=\frac{1}{4}\frac{\lambda^2}{(\gamma-1)^2+\lambda^2}. \tag{E9}$$

Appendix F. Mandel Q function

The first subsection presents the analytical expression for the *initial* Mandel Q function in the matter subsystem, $Q_{\mathrm{mat}}(0)$ in Scheme I and II. The following subsections discuss the impact of the diamagnetic term and the RWA on photon Q function.

F.1. Initial Q_{mat} function in scheme I

To obtain the analytical expression for the initial Mandel Q function of the matter state, $Q_{\mathrm{mat}}(0)$ in Scheme I (i.e. for a shifted by X_0 and squeezed in X Gaussian), we use the formulas for $\langle\hat{n}\rangle$ and $\langle(\Delta\hat{n})^2\rangle$ in equations (7.100) and (7.102) in [79]

$$\langle\hat{n}\rangle=|\alpha|^2+\sinh^2 r,\quad \langle(\Delta\hat{n})^2\rangle=|\alpha|^2e^{2r}+2\sinh^2 r\cosh^2 r. \tag{F1}$$

For the considered Gaussian initial state, $|\alpha|^2=X_0^2/2$ and $r=-\ln(w)$. Substitution yields

$$Q_{\mathrm{mat}}(0)\equiv\frac{\langle(\Delta\hat{n})^2\rangle-\langle\hat{n}\rangle}{\langle\hat{n}\rangle}=\frac{\left(w^2-1\right)^2\left(w^4+1\right)+4w^4\left(w^2-1\right)X_0^2}{4w^4X_0^2+2w^2\left(w^2-1\right)^2}. \tag{F2}$$

Expanding in powers of X_0^{-2}, yields

$$Q_{\mathrm{mat}}(0)=\left(w^2-1\right)-\frac{\left(w^2-1\right)^2\left(w^4-2w^2-1\right)}{4w^4X_0^2}+\mathcal{O}\left(X_0^{-4}\right). \tag{F3}$$

Thus, we obtain the expression used in the main text, $Q_{\mathrm{mat}}(0)=(w^2-1)[1+\mathcal{O}(X_0^{-2})]$.

F.2. Diamagnetic term and RWA in scheme I

For an initially squeezed matter CM state, the photon Q function may attain negative values even in the absence of the diamagnetic term proportional to λ^2 i.e. with the Hamiltonian

$$\hat{\mathcal{H}}^{(1)}=\left[\hat{b}^\dagger\hat{b}+\frac{1}{2}\right]+\gamma\left[\hat{a}^\dagger\hat{a}+\frac{1}{2}\right]-\mathrm{i}\frac{\lambda}{2}\left(\hat{b}^\dagger-\hat{b}\right)\left(\hat{a}^\dagger+\hat{a}\right). \tag{F4}$$

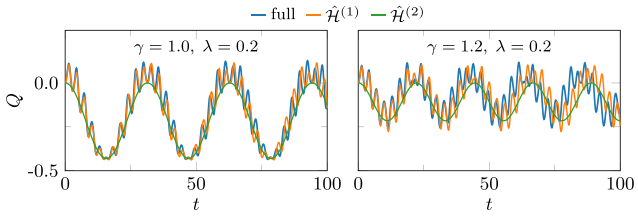

Figure 14. Photon Q function in Scheme I obtained by direct numerical solution of the Schrödinger equation with the HH in equation (15) vs $\hat{\mathcal{H}}^{(1,2)}$ in equations (F4) and (F5). Initial matter state parameters: $X_0 = 3$, $w = 0.5$.

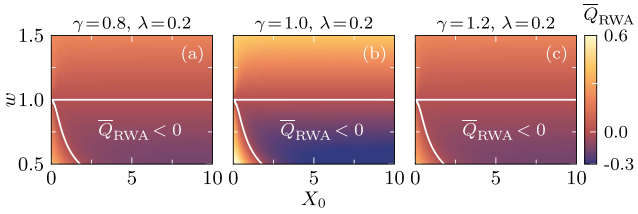

Figure 15. The dependence of photon $\overline{Q}$ on the initial displacement and width of the matter CM X quadrature under RWA. In contrast to figures 6(c)–(e), the pictures on either side of the resonance are identical here.

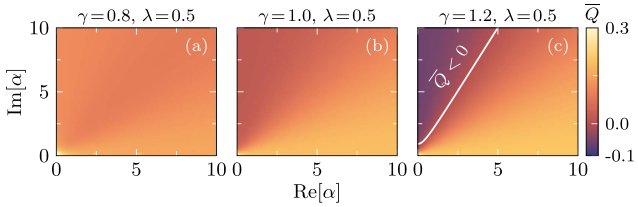

Figure 16. The dependence of photon $\overline{Q}$ on the initial coherent state of the cavity field. Sub-Poissonian PND is achieved off-resonance, and the effect is sensitive to the phase of α. In the ultra-strong coupling regime considered here, $\overline{Q} < 0$ is completely absent in the red-shifted cavity. The negativity saturates with an increasing imaginary component of α.

Under the RWA, i.e. with the Hamiltonian

$$\hat{\mathcal{H}}^{(2)} = \left[\hat{b}^\dagger\hat{b} + \frac{1}{2}\right] + \gamma\left[\hat{a}^\dagger\hat{a} + \frac{1}{2}\right] - \mathrm{i}\frac{\lambda}{2}\hat{b}^\dagger\hat{a} + \mathrm{i}\frac{\lambda}{2}\hat{b}\hat{a}^\dagger, \tag{F5}$$

the effective transfer of nonclassical matter state into the cavity mode is still possible. Figure 14 compares the photon Q functions obtained with the HH vs $\hat{\mathcal{H}}^{(1,2)}$. To isolate the ultrastrong coupling effect, we reproduce figures 6(c)–(e) in figure 15 but under RWA Hamiltonian. $\overline{Q}_{\rm RWA}$ is insensitive to the sign of the relative detuning $(\gamma - 1)$, i.e. panels (a) and (c) are identical. In contrast, panels (c) and (e) in figure 6 exhibit asymmetry induced by the terms omitted in the RWA.

F.3. Diamagnetic term and RWA in scheme II

Figure 16 shows additional examples of the constant component of the photon Q function, $\overline{Q}$ in Scheme II for a range of initial coherent states of the cavity, $|\alpha\rangle$. In this example of the ultra-strong coupling regime, the asymmetry between the red and blue shifted cavities is so pronounced that negative $\overline{Q}$ is obtained only on one side, for $\gamma = 1.2$.

The coherent initial state of the cavity used in Scheme II is not squeezed, i.e. $Q(t = 0) = 0$. Therefore, the counter-rotating terms are essential for generating squeezing and achieving $Q < 0$. Figure 17 shows that under the RWA (i.e. with $\hat{\mathcal{H}}^{(2)}$ in equation (F5)), Q remains zero throughout the motion. In contrast, neglecting the diamagnetic terms (i.e. with $\hat{\mathcal{H}}^{(1)}$ in equation (F4)) produce qualitatively similar results to the full Hamiltonian with negative (on average) photon Q function. Figure 18 focuses on the asymmetry of $\overline{Q}$

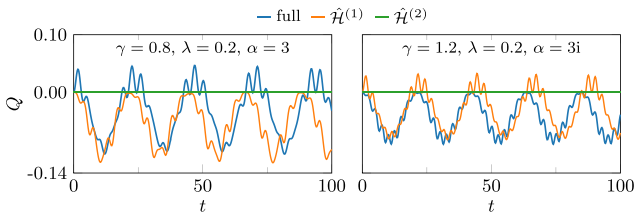

Figure 17. Photon Q function in Scheme II obtained by direct numerical solution of the Schrödinger equation with the HH in equation (15) vs $\hat{\mathcal{H}}^{(1,2)}$ in equations (F4) and (F5).

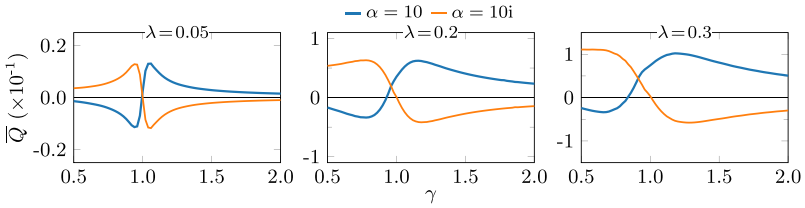

Figure 18. Dependence of the constant component of the photon Q function, $\overline{Q}$ on γ for real/imaginary α, defining the initial coherent state, $|\alpha\rangle$. The chosen values of α are sufficiently high so that $\overline{Q}$ is saturated and no longer changes with increasing α.

about the point of resonance ($\gamma = 1$). Consistent with figure 9, the asymmetry between initial coherent states, $|\alpha\rangle$ with real or imaginary α increases with λ.

ORCID iDs

Ilia Tutunnikov https://orcid.org/0000-0002-8291-7335
Vasil Rokaj https://orcid.org/0000-0002-0627-7292
Jianshu Cao https://orcid.org/0000-0001-7616-7809
H R Sadeghpour https://orcid.org/0000-0001-5707-8675

References

[1] Basov D N, Asenjo-Garcia A, Schuck P J, Zhu X and Rubio A 2021 Polariton panorama *Nanophotonics* **10** 549
[2] Carusotto I and Ciuti C 2013 Quantum fluids of light *Rev. Mod. Phys.* **85** 299
[3] Kockum A F, Miranowicz A, De Liberato S, Savasta S and Nori F 2019 Ultrastrong coupling between light and matter *Nat. Rev. Phys.* **1** 19
[4] Forn-Díaz P, Lamata L, Rico E, Kono J and Solano E 2019 Ultrastrong coupling regimes of light-matter interaction *Rev. Mod. Phys.* **91** 025005
[5] Appugliese F, Enkner J, Paravicini-Bagliani G L, Beck M, Reichl C, Wegscheider W, Scalari G, Ciuti C and Faist J 2022 Breakdown of topological protection by cavity vacuum fields in the integer quantum Hall effect *Science* **375** 1030
[6] Enkner J, Graziotto L, Appugliese F, Rokaj V, Wang J, Ruggenthaler M, Reichl C, Wegscheider W, Rubio A and Faist J 2024 Testing the renormalization of the von Klitzing constant by cavity vacuum fields *Phys. Rev.* X **14** 021038
[7] Hagenmüller D, De Liberato S and Ciuti C 2010 Ultrastrong coupling between a cavity resonator and the cyclotron transition of a two-dimensional electron gas in the case of an integer filling factor *Phys. Rev.* B **81** 235303
[8] Scalari G *et al* 2012 Ultrastrong coupling of the cyclotron transition of a 2D electron gas to a THz metamaterial *Science* **335** 1323
[9] Bayer A, Pozimski M, Schambeck S, Schuh D, Huber R, Bougeard D and Lange C 2017 Terahertz light-matter interaction beyond unity coupling strength *Nano Lett.* **17** 6340
[10] Ravets S, Knüppel P, Faelt S, Cotlet O, Kroner M, Wegscheider W and Imamoğlu A 2018 Polaron polaritons in the integer and fractional quantum Hall regimes *Phys. Rev. Lett.* **120** 057401
[11] Sentef M A, Ruggenthaler M and Rubio A 2018 Cavity quantum-electrodynamical polaritonically enhanced electron-phonon coupling and its influence on superconductivity *Sci. Adv.* **4** eaau6969
[12] Li X, Bamba M, Zhang Q, Fallahi S, Gardner G C, Gao W, Lou M, Yoshioka K, Manfra M J and Kono J 2018 Vacuum Bloch-Siegert shift in Landau polaritons with ultra-high cooperativity *Nat. Photon.* **12** 324
[13] Schlawin F, Cavalleri A and Jaksch D 2019 Cavity-mediated electron-photon superconductivity *Phys. Rev. Lett.* **122** 133602
[14] Curtis J B, Raines Z M, Allocca A A, Hafezi M and Galitski V M 2019 Cavity quantum Eliashberg enhancement of superconductivity *Phys. Rev. Lett.* **122** 167002
[15] Rokaj V, Wang J, Sous J, Penz M, Ruggenthaler M and Rubio A 2023 Weakened topological protection of the quantum Hall effect in a cavity *Phys. Rev. Lett.* **131** 196602
[16] Schlawin F, Kennes D M and Sentef M A 2022 Cavity quantum materials *Appl. Phys. Rev.* **9** 011312
[17] Kasprzak J *et al* 2006 Bose-Einstein condensation of exciton polaritons *Nature* **443** 409

[18] Dudin Y O and Kuzmich A 2012 Strongly interacting Rydberg excitations of a cold atomic gas *Science* **336** 887
[19] Peyronel T, Firstenberg O, Liang Q-Y, Hofferberth S, Gorshkov A V, Pohl T, Lukin M D and Vuletić V 2012 Quantum nonlinear optics with single photons enabled by strongly interacting atoms *Nature* **488** 57
[20] Mivehvar F, Piazza F, Donner T and Ritsch H 2021 Cavity QED with quantum gases: new paradigms in many-body physics *Adv. Phys.* **70** 1
[21] Hutchison J A, Schwartz T, Genet C, Devaux E and Ebbesen T W 2012 Modifying chemical landscapes by coupling to vacuum fields *Angew. Chem., Int. Ed.* **51** 1592
[22] Ebbesen T W 2016 Hybrid light-matter states in a molecular and material science perspective *Acc. Chem. Res.* **49** 2403
[23] George J, Chervy T, Shalabney A, Devaux E, Hiura H, Genet C and Ebbesen T W 2016 Multiple Rabi splittings under ultrastrong vibrational coupling *Phys. Rev. Lett.* **117** 153601
[24] Yang P-Y and Cao J 2021 Quantum effects in chemical reactions under polaritonic vibrational strong coupling *J. Phys. Chem. Lett* **12** 9531
[25] Wu A, Cerrillo J and Cao J 2024 Extracting kinetic information from short-time trajectories: relaxation and disorder of lossy cavity polaritons *Nanophotonics* **13** 2575
[26] Sidler D, Ruggenthaler M, Schäfer C, Ronca E and Rubio A 2022 A perspective on *ab initio* modeling of polaritonic chemistry: the role of non-equilibrium effects and quantum collectivity *J. Chem. Phys.* **156** 230901
[27] Feist J, Galego J and Garcia-Vidal F J 2018 Polaritonic chemistry with organic molecules *ACS Photon.* **5** 205
[28] Hou S, Khatoniar M, Ding K, Qu Y, Napolov A, Menon V M and Forrest S R 2020 Ultralong-range energy transport in a disordered organic semiconductor at room temperature via coherent exciton-polariton propagation *Adv. Mater.* **32** 2002127
[29] Keeling J and Kéna-Cohen S 2020 Bose-Einstein condensation of exciton-polaritons in organic microcavities *Annu. Rev. Phys. Chem.* **71** 435
[30] Garcia-Vidal F J, Ciuti C and Ebbesen T W 2021 Manipulating matter by strong coupling to vacuum fields *Science* **373** eabd0336
[31] Balasubrahmaniyam M, Simkhovich A, Golombek A, Sandik G, Ankonina G and Schwartz T 2023 From enhanced diffusion to ultrafast ballistic motion of hybrid light-matter excitations *Nat. Mat.* **22** 338
[32] Kuhn A, Hennrich M and Rempe G 2002 Deterministic single-photon source for distributed quantum networking *Phys. Rev. Lett.* **89** 067901
[33] Andersen U L, Gehring T, Marquardt C and Leuchs G 2016 30 years of squeezed light generation *Phys. Scr.* **91** 053001
[34] Law C K 1995 Interaction between a moving mirror and radiation pressure: a Hamiltonian formulation *Phys. Rev.* A **51** 2537
[35] Aspelmeyer M, Kippenberg T J and Marquardt F 2014 Cavity optomechanics *Rev. Mod. Phys.* **86** 1391
[36] Safavi-Naeini A H, Gröblacher S, Hill J T, Chan J, Aspelmeyer M and Painter O 2013 Squeezed light from a silicon micromechanical resonator *Nature* **500** 185
[37] Purdy T P, Yu P-L, Peterson R W, Kampel N S and Regal C A 2013 Strong optomechanical squeezing of light *Phys. Rev.* X **3** 031012
[38] Brooks D W C, Botter T, Schreppler S, Purdy T P, Brahms N and Stamper-Kurn D M 2012 Non-classical light generated by quantum-noise-driven cavity optomechanics *Nature* **488** 476
[39] Takahashi H, Kassa E, Christoforou C and Keller M 2020 Strong coupling of a single ion to an optical cavity *Phys. Rev. Lett.* **124** 013602
[40] Rokaj V, Mistakidis S I and Sadeghpour H R 2023 Cavity induced collective behavior in the polaritonic ground state *SciPost Phys.* **14** 167
[41] Hopfield J J 1958 Theory of the contribution of excitons to the complex dielectric constant of crystals *Phys. Rev.* **112** 1555
[42] Rokaj V, Welakuh D M, Ruggenthaler M and Rubio A 2018 Light–matter interaction in the long-wavelength limit: no ground-state without dipole self-energy *J. Phys. B: At. Mol. Opt. Phys.* **51** 034005
[43] Spohn H 2004 *Dynamics of Charged Particles and Their Radiation Field* (Cambridge University Press) (https://doi.org/10.1017/CBO9780511535178)
[44] Kreuter A, Becher C, Lancaster G P T, Mundt A B, Russo C, Häffner H, Roos C, Eschner J, Schmidt-Kaler F and Blatt R 2004 Spontaneous emission lifetime of a single trapped Ca^+ ion in a high finesse cavity *Phys. Rev. Lett.* **92** 203002
[45] Stute A, Casabone B, Brandstätter B, Habicher D, Barros H G, Schmidt P O, Northup T E and Blatt R 2012 Toward an ion-photon quantum interface in an optical cavity *Appl. Phys.* B **107** 1145
[46] Takahashi H, Kassa E, Christoforou C and Keller M 2017 Cavity-induced anticorrelated photon-emission rates of a single ion *Phys. Rev.* A **96** 023824
[47] Keller M 2022 Cavity-QED with single trapped ions *Contemp. Phys.* **63** 1
[48] Guthöhrlein G R, Keller M, Hayasaka K, Lange W and Walther H 2001 A single ion as a nanoscopic probe of an optical field *Nature* **414** 49
[49] Meekhof D M, Monroe C, King B E, Itano W M and Wineland D J 1996 Generation of nonclassical motional states of a trapped atom *Phys. Rev. Lett.* **76** 1796
[50] Boozer A D, Boca A, Miller R, Northup T E and Kimble H J 2007 Reversible state transfer between light and a single trapped atom *Phys. Rev. Lett.* **98** 193601
[51] Stute A, Casabone B, Brandstätter B, Friebe K, Northup T E and Blatt R 2013 Quantum-state transfer from an ion to a photon *Nat. Photon.* **7** 219
[52] Hite D A, Colombe Y, Wilson A C, Allcock D T C, Leibfried D, Wineland D J and Pappas D P 2013 Surface science for improved ion traps *MRS Bull.* **38** 826
[53] Smolka S, Wuester W, Haupt F, Faelt S, Wegscheider W and Imamoğlu A 2014 Cavity quantum electrodynamics with many-body states of a two-dimensional electron gas *Science* **346** 332
[54] Paravicini-Bagliani G L *et al* 2019 Magneto-transport controlled by Landau polariton states *Nat. Phys.* **15** 186
[55] Keller J *et al* 2020 Landau polaritons in highly nonparabolic two-dimensional gases in the ultrastrong coupling regime *Phys. Rev.* B **101** 075301
[56] Rokaj V, Penz M, Sentef M A, Ruggenthaler M and Rubio A 2019 Quantum electrodynamical Bloch theory with homogeneous magnetic fields *Phys. Rev. Lett.* **123** 047202
[57] Rokaj V 2022 Condensed matter systems in cavity quantum electrodynamics (arXiv:2201.01331 [quant-ph])
[58] Ciuti C 2021 Cavity-mediated electron hopping in disordered quantum Hall systems *Phys. Rev.* B **104** 155307
[59] Rokaj V, Penz M, Sentef M A, Ruggenthaler M and Rubio A 2022 Polaritonic Hofstadter butterfly and cavity control of the quantized Hall conductance *Phys. Rev.* B **105** 205424
[60] Thomas A *et al* 2016 Ground-state chemical reactivity under vibrational coupling to the vacuum electromagnetic field *Angew. Chem.* **55** 11462

[61] Lather J, Bhatt P, Thomas A, Ebbesen T W and George J 2019 Cavity catalysis by cooperative vibrational strong coupling of reactant and solvent molecules *Angew. Chem., Int. Ed.* **58** 10635
[62] Thomas A *et al* 2019 Tilting a ground-state reactivity landscape by vibrational strong coupling *Science* **363** 615
[63] Sun K and Ribeiro R F 2024 Theoretical formulation of chemical equilibrium under vibrational strong coupling *Nat. Commun.* **15** 2405
[64] Xiang B and Xiong W 2024 Molecular polaritons for chemistry, photonics and quantum technologies *Chem. Rev.* **124** 2512
[65] Freixanet T, Sermage B, Tiberj A and Planel R 2000 In-plane propagation of excitonic cavity polaritons *Phys. Rev.* B **61** 7233
[66] Orgiu E *et al* 2015 Conductivity in organic semiconductors hybridized with the vacuum field *Nat. Mater.* **14** 1123
[67] Pandya R *et al* 2021 Microcavity-like exciton-polaritons can be the primary photoexcitation in bare organic semiconductors *Nat. Commun.* **12** 6519
[68] Engelhardt G and Cao J 2022 Unusual dynamical properties of disordered polaritons in microcavities *Phys. Rev.* B **105** 064205 Engelhardt G and Cao J 2023 Polariton localization and dispersion properties of disordered quantum emitters in multimode microcavities *Phys. Rev. Lett.* **130** 213602
[69] Sokolovskii I, Tichauer R H, Morozov D, Feist J and Groenhof G 2023 Multi-scale molecular dynamics simulations of enhanced energy transfer in organic molecules under strong coupling *Nat. Commun.* **14** 6613
[70] Aroeira G J R, Kairys K T and Ribeiro R F 2024 Coherent transient exciton transport in disordered polaritonic wires *Nanophotonics* **13** 2553
[71] Zhou Z, Chen H-T, Sukharev M, Subotnik J E and Nitzan A 2024 Nature of polariton transport in a Fabry-Perot cavity *Phys. Rev.* A **109** 033717
[72] Sandik G, Feist J, García-Vidal F J and Schwartz T 2024 Cavity-enhanced energy transport in molecular systems *Nat. Mater.* (https://doi.org/10.1038/s41563-024-01962-5)
[73] Li T E, Nitzan A and Subotnik J E 2020 On the origin of ground-state vacuum-field catalysis: equilibrium consideration *J. Chem. Phys.* **152** 234107
[74] Ruggenthaler M, Sidler D and Rubio A 2023 Understanding polaritonic chemistry from *ab initio* quantum electrodynamics *Chem. Rev.* **123** 11191
[75] Campos-Gonzalez-Angulo J A, Poh Y R, Du M and Yuen-Zhou J 2023 Swinging between shine and shadow: theoretical advances on thermally activated vibropolaritonic chemistry *J. Chem. Phys.* **158** 230901
[76] Mandal A, Taylor M A D, Weight B M, Koessler E R, Li X and Huo P 2023 Theoretical advances in polariton chemistry and molecular cavity quantum electrodynamics *Chem. Rev.* **123** 9786
[77] Fiechter M R, Runeson J E, Lawrence J E and Richardson J O 2023 How quantum is the resonance behavior in vibrational polariton chemistry? *J. Phys. Chem. Lett.* **14** 8261
[78] Schwennicke K, Koner A, Pérez-Sánchez J B, Xiong W, Giebink N C, Weichman M L and Yuen-Zhou J 2024 When do molecular polaritons behave like optical filters? (arXiv:2408.05036 [physics.chem-ph])
[79] Gerry C and Knight P 2012 *Introductory Quantum Optics* (Cambridge University Press) (https://doi.org/10.1017/CBO9780511791239)
[80] Welakuh D M, Tserkis S, Smart S E and Narang P 2024 Cavity-mediated molecular entanglement and generation of non-classical states of light *J. Phys. Chem.* A **128** 799
[81] Brune M, Schmidt-Kaler F, Maali A, Dreyer J, Hagley E, Raimond J M and Haroche S 1996 Quantum Rabi oscillation: a direct test of field quantization in a cavity *Phys. Rev. Lett.* **76** 1800
[82] Law C K and Kimble H J 1997 Deterministic generation of a bit-stream of single-photon pulses *J. Mod. Opt.* **44** 2067
[83] Degen C L, Reinhard F and Cappellaro P 2017 Quantum sensing *Rev. Mod. Phys.* **89** 035002
[84] Gleyzes S, Kuhr S, Guerlin C, Bernu J, Deléglise S, Busk Hoff U, Brune M, Raimond J-M and Haroche S 2007 Quantum jumps of light recording the birth and death of a photon in a cavity *Nature* **446** 297
[85] Facon A, Dietsche E-K, Grosso D, Haroche S, Raimond J-M, Brune M and Gleyzes S 2016 A sensitive electrometer based on a Rydberg atom in a Schrödinger-cat state *Nature* **535** 262
[86] Xie T *et al* 2021 Beating the standard quantum limit under ambient conditions with solid-state spins *Sci. Adv.* **7** eabg9204
[87] Gao W-B, Lu C-Y, Yao X-C, Xu P, Gühne O, Goebel A, Chen Y-A, Peng C-Z, Chen Z-B and Pan J-W 2010 Experimental demonstration of a hyper-entangled ten-qubit Schrödinger cat state *Nat. Phys.* **6** 331
[88] Lib O and Bromberg Y 2024 Resource-efficient photonic quantum computation with high-dimensional cluster states *Nat. Photon.* **18** 1218–24
[89] Cohen-Tannoudji C, Dupont-Roc J and Grynberg G 1997 *Photons and Atoms: Introduction to Quantum Electrodynamics* (Wiley) (https://doi.org/10.1002/9783527618422)
[90] Busch T, Englert B-G, Rzażewski K and Wilkens M 1998 Two cold atoms in a harmonic trap *Found. Phys.* **28** 549
[91] Schäfer C, Ruggenthaler M, Rokaj V and Rubio A 2020 Relevance of the quadratic diamagnetic and self-polarization terms in cavity quantum electrodynamics *ACS Photon.* **7** 975
[92] Horak J, Sidler D, Huang W-M, Ruggenthaler M and Rubio A 2024 Analytic model for molecules under collective vibrational strong coupling in optical cavities (arXiv:2401.16374 [quant-ph])
[93] Pannir-Sivajothi S, Campos-Gonzalez-Angulo J A, Martínez-Martínez L A, Sinha S and Yuen-Zhou J 2022 Driving chemical reactions with polariton condensates *Nat. Commun.* **13** 1645
[94] Kristensen P T, Vlack C V and Hughes S 2012 Generalized effective mode volume for leaky optical cavities *Opt. Lett.* **37** 1649
[95] Shankar R 1994 *Principles of Quantum Mechanics* 2nd edn (Springer) (available at: https://link.springer.com/book/10.1007/978-1-4757-0576-8)
[96] Tannor D 2007 *Introduction to Quantum Mechanics: A Time-Dependent Perspective* 1st edn (University Science Books) (available at: https://uscibooks.aip.org/books/introduction-to-quantum-mechanics-a-time-dependent-perspective/)
[97] Laughlin R B 1981 Quantized Hall conductivity in two dimensions *Phys. Rev.* B **23** 5632
[98] Li Q P, Karraï K, Yip S K, Das Sarma S and Drew H D 1991 Electrodynamic response of a harmonic atom in an external magnetic field *Phys. Rev.* B **43** 5151
[99] Deimert C, Goulain P, Manceau J-M, Pasek W, Yoon T, Bousseksou A, Kim N Y, Colombelli R and Wasilewski Z R 2020 Realization of harmonic oscillator arrays with graded semiconductor quantum wells *Phys. Rev. Lett.* **125** 097403
[100] Banin U, Bartana A, Ruhman S and Kosloff R 1994 Impulsive excitation of coherent vibrational motion ground surface dynamics induced by intense short pulses *J. Chem. Phys* **101** 8461
[101] Shapiro M and Brumer P 2011 *Quantum Control of Molecular Processes* (Wiley) (https://doi.org/10.1002/9783527639700)
[102] Mandel L 1979 Sub-Poissonian photon statistics in resonance fluorescence *Opt. Lett.* **4** 205

[103] Welakuh D M, Ruggenthaler M, Tchenkoue M-L M, Appel H and Rubio A 2021 Down-conversion processes in *ab initio* nonrelativistic quantum electrodynamics *Phys. Rev. Res.* **3** 033067
[104] Walls D F and Milburn G J 2008 *Quantum Optics* (Springer) (https://doi.org/10.1007/978-3-540-28574-8)
[105] Rempe G, Thompson R J, Brecha R J, Lee W D and Kimble H J 1991 Optical bistability and photon statistics in cavity quantum electrodynamics *Phys. Rev. Lett.* **67** 1727
[106] Gardiner C W and Collett M J 1985 Input and output in damped quantum systems: quantum stochastic differential equations and the master equation *Phys. Rev.* A **31** 3761
[107] Lindoy L P, Mandal A and Reichman D R 2024 Investigating the collective nature of cavity-modified chemical kinetics under vibrational strong coupling *Nanophotonics* **13** 2617